RESEARCH ARTICLE

The Organization of Controller Motifs Leading to Robust Plant Iron Homeostasis

Oleg Agafonov[1], Christina Helen Selstø[1], Kristian Thorsen[2], Xiang Ming Xu[1], Tormod Drengstig[2], Peter Ruoff[1] *

1 Centre for Organelle Research, University of Stavanger, Stavanger, Norway, 2 Department of Electrical Engineering and Computer Science, University of Stavanger, Stavanger, Norway

* peter.ruoff@uis.no

Abstract

Iron is an essential element needed by all organisms for growth and development. Because iron becomes toxic at higher concentrations iron is under homeostatic control. Plants face also the problem that iron in the soil is tightly bound to oxygen and difficult to access. Plants have therefore developed special mechanisms for iron uptake and regulation. During the last years key components of plant iron regulation have been identified. How these components integrate and maintain robust iron homeostasis is presently not well understood. Here we use a computational approach to identify mechanisms for robust iron homeostasis in non-graminaceous plants. In comparison with experimental results certain control arrangements can be eliminated, among them that iron homeostasis is solely based on an iron-dependent degradation of the transporter IRT1. Recent IRT1 overexpression experiments suggested that IRT1-degradation is iron-independent. This suggestion appears to be misleading. We show that iron signaling pathways under IRT1 overexpression conditions become saturated, leading to a breakdown in iron regulation and to the observed iron-independent degradation of IRT1. A model, which complies with experimental data places the regulation of cytosolic iron at the transcript level of the transcription factor *FIT*. Including the experimental observation that FIT induces inhibition of IRT1 turnover we found a significant improvement in the system's response time, suggesting a functional role for the FIT-mediated inhibition of IRT1 degradation. By combining iron uptake with storage and remobilization mechanisms a model is obtained which in a concerted manner integrates iron uptake, storage and remobilization. In agreement with experiments the model does not store iron during its high-affinity uptake. As an iron biofortification approach we discuss the possibility how iron can be accumulated even during high-affinity uptake.

Introduction

Iron is an essential element required by all organisms, but becomes toxic at higher levels. Iron is needed as a cofactor for many enzymes and proteins. To provide a sufficient level of available iron in the cytosol without leading to toxicity, iron is under homeostatic control. Plants have

also the problem that iron in the soil under aerobic conditions is generally present as low-soluble iron(III)-oxide forms which require a high-affinity transport system for its uptake. To cope with these difficulties plants have developed two main strategies for iron-uptake, one termed strategy I for non-graminaceous plants (plants not belonging to the grass family) and the other termed strategy II for graminaceous plants [1]. During recent years considerable advances have been made to identify molecular components of the iron uptake and storage mechanisms [2–7]. In this work we focus on iron regulation of strategy I plants which includes the model plant *Arabidopsis thaliana*. Fig 1 gives an overview of the iron flow, storage, and regulatory components in these plants. IRT1 has been identified as the major transporter responsible for the high-affinity uptake of iron from the soil [8–10].

Prior to the uptake of iron(II) by IRT1, iron(III)'s solubility in the soil is increased by secreting H^+ using H^+-ATPases followed by the reduction of iron(III) to iron(II) by a membrane-bound ferric reductase oxidase (FRO2). The helix-loop-helix (bHLH) transcription factor FIT [11] has been found to be required for the iron deficiency response in Arabidopsis, where several iron regulated genes appear under the control of FIT [12]. FIT interacts with two other bHLH proteins, AtbHLH38 and AtbHLH39, where the transcription of *FRO2* and *IRT1* are regulated by FIT/AtbHLH38 and FIT/AtbHLH39 [13]. Once inside the cell, iron(II) is complexed and buffered by several organic compounds, among them Nicotianamine (NA), which is considered to stabilize predominantly Fe(II) but also Fe(III) [14] and appears to be an important transport form of iron in all plants [15–19].

By using *IRT1* knockout plants Vert et al. [10] observed that IRT1 is necessary for plant survival in the presence of low external iron levels, but that the absence of IRT1 plants can be counteracted by adding iron into the watering solution.

In accordance with results from metal-ion homeostasis in yeast [20], Connolly et al. [21] suggested a homeostasis-mediating mechanism based on the iron-dependent degradation of IRT1, where the amino acids K164 or K171 in IRT1 have been found to be necessary for IRT1 turnover [22]. This suggestion is supported by experiments [21] showing that the level of IRT1 (and its transcript) is high at low external iron concentrations, but declines once plants are transferred to sufficient iron conditions. In further agreement with an iron-dependent IRT1-degradation mechanism, 35S-*IRT1* plants which overexpress IRT1 in an Arabidopsis wild-type background have higher *IRT1* transcript levels, while protein levels were low and comparable to wild-type plants [22].

Barberon et al. [23] observed that overexpression of IRT1 in an *IRT1*-knockout background leads to elevated iron levels and toxicity. Furthermore, the IRT1 degradation rate under such conditions was found to be independent of the actual iron supply, in contrast to the earlier suggestion by Connolly et al. [21] of an iron-dependent degradation of IRT1. Despite the discrepancy whether IRT1 is subject to an iron-dependent degradation or not, there is a consensus that in roots mRNA and protein levels of *IRT1* and *FIT* are inversely correlated to the amount of external iron [10, 12, 21–23]. In other words, a sufficient supply of iron leads to low levels of *IRT1* and *FIT* transcripts and low levels of the corresponding proteins. Decreased supply levels of iron result in the up-regulation of both the *IRT1/FIT* transcripts and the corresponding proteins.

Chloroplasts require large amounts of iron due to photosynthesis, heme biosynthesis and Fe-S cluster synthesis. Besides chloroplasts, also mitochondria have a large demand for iron due to iron-containing respiratory enzymes. It is therefore expected that also these iron-requiring organelles have mechanisms to maintain iron homeostasis. Comparative studies of determined iron levels in roots and leaves performed with different wild-type and mutant plants show that roots have generally an iron content which is approximately one order of magnitude higher than in leaves (S1 Table). This indicates that in roots protective and homeostatic
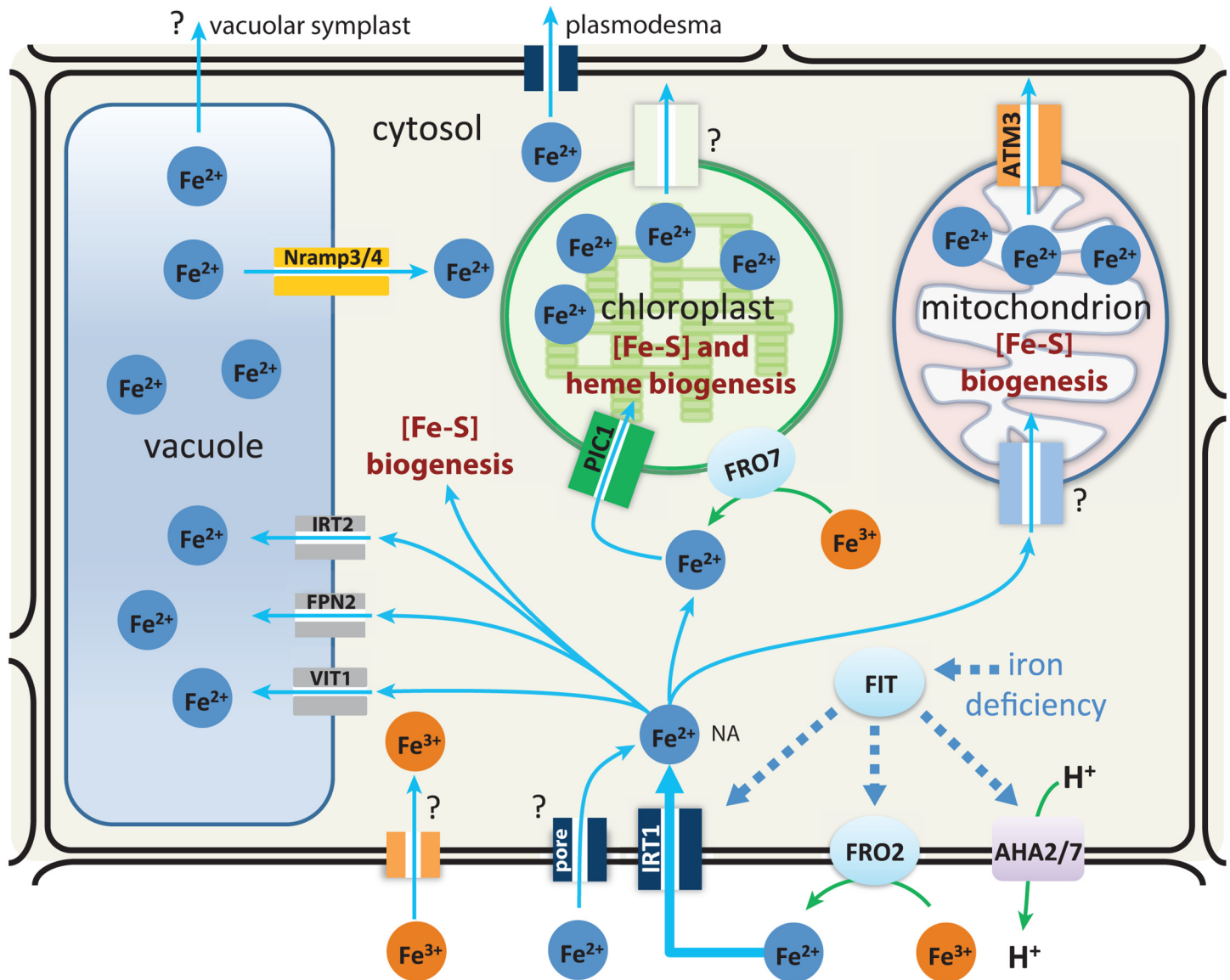
Fig 1. Regulatory components of iron homeostasis in non-graminaceous plant cells. In the presence of iron deficiency the transcription factor FIT activates the excretion of H^+ by ATPases AHA2/7, which leads to an increased solubility of Fe(III). FIT also induces the reduction of solubilized Fe(III) to Fe(II) by the membrane-bound enzyme FRO2 and activates the high-affinity transporter IRT1 and the uptake of Fe(II). Iron is stored in different organelles with the vacuole as a major store. Several transporters which move iron into organelles and the vacuole have been identified (see main text). Iron transport to other parts of the plant occurs in complexed form with the water flow, i.e. via the cytosolic symplast connected by plasmodesmata and perhaps also by a transport route using a vacuolar symplast. Transporter candidates for iron remobilization from the store are Nramp3/4.

doi:10.1371/journal.pone.0147120.g001

mechanisms need to be present in order to avoid iron toxicity while delivering iron to other parts of the plant.

The aim of this work is to rationalize, in agreement with experimental results, the organization of controller motifs, which lead to robust iron homeostasis in root cells during iron uptake, its assimilation and transport to other parts of the plant, as well as iron storage and its remobilization from the store. Before dealing with the aspects of iron regulation we give an overview of the concept of integral control, its importance for robust homeostasis and the kinetic implementations which lead to integral control in biochemical systems.

Kinetic Requirements for Robust Homeostasis

The term *homeostasis* was introduced by Cannon in 1929 [24]. According to Cannon's definition homeostasis maintains the steady states of compounds in an organism/cell at approximately constant and stable levels, where variations of these compounds may occur within certain but narrow limits [24–26]. Homeostasis is a concept which is closely related to the internal stability of organisms and cells [27]. Langley [26] provided an interesting compilation of key contributions which led to the development of the concept.

In control engineering it is well established that *integral control* (see e.g. [28]), as part of a negative feedback loop, will keep the level of a certain variable precisely at a given set-point even in the presence of environmental perturbations. Although the concept of integral control has extensively been used in industrial control processes since the last century its relevance with respect to the regulation of biochemical processes in organisms and cells was only relative recently pointed out [29] and studied in relation to several homeostatic processes [30–39].

We have been studying the kinetic requirements which lead to integral control in biochemical systems containing a negative feedback [33, 37, 38] including an extension of the homeostasis concept to oscillatory conditions [40]. To illustrate the effect of negative feedback regulation on a compound *A* consider the process:

$$\xrightarrow{k_1} A \xrightarrow{k_2} \tag{1}$$

where k_1 and k_2 are rate constants describing the inflow and outflow of *A* according to the rate equation:

$$\dot{A} = k_1 - k_2 \cdot A \tag{2}$$

Because the steady state level of *A* depends both on k_1 and k_2, i.e., $A_{ss} = k_1/k_2$, it is obvious that A_{ss} is not under homeostatic control.

To keep the level of *A* at a certain set-point A_{set}, integral control is invoked as part of a negative feedback controller loop. In integral control (Fig 2a) the difference (error *e*) between the actual value of *A* and its set-point A_{set}, is calculated and integrated over time. The integrated error *E* is then used to compensate for perturbations in the concentration of A (for example when k_1 or k_2 are changed by environmental influences), which would drive the level of *A* away from its set-point. The controller loops can be divided into two classes, which we have termed *inflow* and *outflow* controllers [37]. An inflow controller provides a compensatory flux, which *adds A* from some other source to the system when uncontrolled perturbations decrease the level of *A*. In an outflow controller the situation is reversed, i.e., the compensatory flux *removes A* from the system by excreting *A* or moving it to a store [37]. Although a negative feedback loop is necessary to obtain robust homeostasis, negative feedback alone is not sufficient unless integral control is invoked. A justification of this statement is given in S1 Text. To illustrate the kinetic condition that leads to integral control and robust homeostasis, Fig 2b shows an inflow controller (motif 1, Ref. [37]), where integral control is implemented by an enzyme termed E_{set}, which removes *E* under close to saturation conditions (low $K_M^{E_{set}}$ value). The name E_{set} reflects the enzyme's importance for determining the set-point of A. The dashed arrows in Fig 2b with positive signs going from *A* to *E* indicate signaling events where *A* activates enzyme E_{set}. In cybernetic terms the signaling from *A* to *E* is termed *measurement* and is part of the *A*-sensing mechanism of the controller. The dashed arrows from *E* to *A* indicate the signaling event where *E* activates the synthesis of *A*. In cybernetic terms this represents the *control input*, which is part of the compensatory mechanism and maintains homeostasis in *A*. For the sake of simplicity we assume here that the signaling events originating from *A* and *E* are proportional
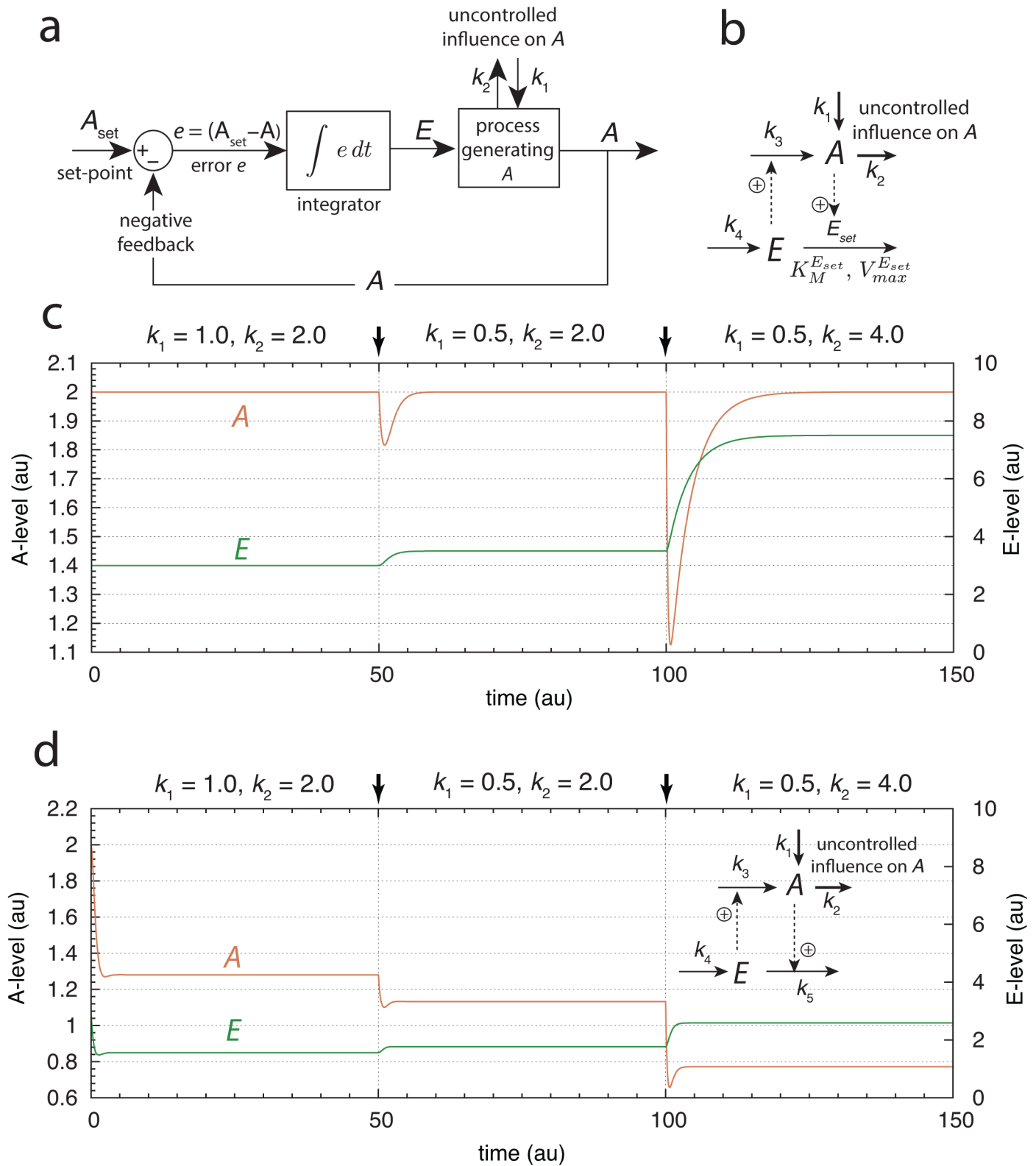
Fig 2. Negative Feedback Loops with and without Integral Control. (a) Flow diagram illustrating the concept of integral control. The regulated value of A is compared with its set-point A_{set} and the integral E of the error e between A and its set-point is calculated. E is fed into the process to compensate uncontrolled inflow or outflow to and from A. (b) Scheme of an inflow controller, where integral control is represented by removing E with enzyme E_{set}, which is

saturated with substrate E and reflected by a low $K_M^{E_{set}}$ value. (c) Illustration of robust homeostasis in A for different k_1, k_2 combinations with set-point $k_4/V_{max}^{E_{set}}$ Eq (6). The change in k_1 and k_2 occurs at $t = 50.0$ and $t = 100.0$ time units indicated by the arrows. Rate constants: $k_3 = 1.0$, $k_4 = 2.0$, $V_{max}^{E_{set}} = 1.0$, and $K_M^{E_{set}} = 1 \times 10^{-4}$. Initial concentrations: $A_0 = 2.0$, and $E_0 = 3.0$. (d) Same negative feedback loop as in (b), but without integral control. The saturating kinetics of the E-removal is now replaced by a first-order process with respect to E with $k_5 = 1.0$. The system is now not able to maintain robust homeostasis in A. Initial concentrations and the other rate constants are as in (c).

to the concentrations of A and E, respectively. The rate equations for A and E are written as:

$$\dot{A} = k_1 + k_3 \cdot E - k_2 \cdot A \tag{3}$$

$$\dot{E} = k_4 - A \cdot \frac{V_{max}^{E_{set}} \cdot E}{K_M^{E_{set}} + E} \tag{4}$$

Eq (4) determines the set-point for A. For $K_M^{E_{set}} \ll E$, the removal of E becomes zero-order with respect to E and Eq (4) simplifies to

$$\dot{E} \approx k_4 - V_{max}^{E_{set}} \cdot A = V_{max}^{E_{set}} \left(\frac{k_4}{V_{max}^{E_{set}}} - A \right) = V_{max}^{E_{set}} (A_{set} - A) \tag{5}$$

We see that $\dot{E}$ is proportional to the error $e = (A_{set} - A)$, and as required by integral control, the concentration of E is proportional to the integrated error (Fig 2a).

Under these conditions, the steady state concentration in A is given as

$$A_{ss} = A_{set} = k_4/V_{max}^{E_{set}} \tag{6}$$

and is independent of k_1 and k_2. Fig 2c illustrates the homeostatic behavior of the system when k_1 and k_2 values are varied.

The inset in Fig 2d shows the same negative feedback structure as in Fig 2b, but without the implementation of an integral controller. The zero-order removal of E in Fig 2b is now replaced by first-order kinetics:

$$\dot{E} = k_4 - k_5 \cdot A \cdot E \tag{7}$$

Because integral control with a defined set-point is lacking the steady state concentration of A (A_{ss}) depends now on all four rate constants:

$$A_{ss} = \frac{k_1 + \sqrt{\frac{k_1^2 \cdot k_5 + 4 \cdot k_2 \cdot k_3 \cdot k_4}{k_5}}}{2 \cdot k_2} \tag{8}$$

Fig 2d shows the numerical results when the same changes in k_1 and k_2 are applied as in Fig 2c, but without integral control. In this case robust homeostasis cannot be maintained, although the steady state value of A for the negative feedback loop alone (Fig 2d) is higher than it would be without any negative feedback. Without a negative feedback the steady state would be $A_{ss} = k_1/k_2$, i.e., 0.5, 0.25 and 0.125 for the three different combinations of k_1 and k_2 in Fig 2d.

As we will show below, a negative feedback without integral control can still significantly affect another integral controller's behavior by improving (decreasing) its response time while keeping the set-point unchanged.

Materials and Methods

The experimental results on mRNA and protein levels we here will refer to have been reported in form of relative grayness levels of gel- and/or Western blots. Because experimentally determined cellular concentrations and associated rate parameters of compounds are still unknown, concentrations, rate constant and parameter values used in the models are kept in arbitrary units (au). However, to make the correspondence between modeling and experimental results as close as possible modeling results are reported, as experiments, in a blot-wise manner where gray levels reflect uncalibrated concentrations. According to the agreed convention in plant molecular biology, mRNAs are referred to in capitalized italic letters, while protein names are written capitalized and non-italic. Plants that had their *IRT1-gene* knocked-out are referred to with small italic letters, i.e. *irt1*. Computations were performed by using the Fortran subroutine LSODE [41] and compared with corresponding Matlab/Simulink calculations. Plots were generated with gnuplot (www.gnuplot.info) and Adobe Illustrator (adobe.com). To make notations simpler, concentrations of compounds are denoted by compound names without square brackets. To make the computational results available, Matlab files are provided as Supporting Information.

Results and Discussion

Negative Feedback with an Iron-dependent IRT1 degradation

We first investigated the suggestion by Connolly et al. [21] that IRT1 is degraded in an iron-dependent manner in comparison with the observation by Barberon et al. [23] that overexpression of IRT1 leads to an iron-independent degradation of IRT1.

To understand these apparently opposing viewpoints we studied the model shown in Fig 3a, where iron homeostasis during iron uptake is based on an iron-dependent removal of the transporter protein IRT1. The inflow control structure of the model (the rate equations are given in S2 Text) is able to maintain homeostasis when the cellular demand for iron is relatively high.

For simplicity, the (high-affinity) uptake rate of iron by IRT1 is described as

$$j_{IRT1}^{Fe-uptake} = k_1 \cdot IRT1 \cdot Fe_{ext} \tag{9}$$

where $j_{IRT1}^{Fe-uptake}$ is proportional to the concentration of the transporter IRT1 and to the concentration of external iron, Fe_{ext}. Because the IRT1-based uptake of iron in general will show saturation kinetics, Eq (9) implies that iron uptake by IRT1 is far from saturation. By using isothermal titration calorimetry Grossoehme et al. [42] found that Fe^{2+} and other IRT1-transported metal-ions show a relative weak binding to IRT1 and that the description by Eq (9) appears approximately valid. To further simplify the model, the flux which maintains the cell's need for iron and the transport flux of iron from the root to other parts of the plant are lumped together and described by the term $j_{Fe-assim}$

$$j_{Fe-assim} = k_2 \cdot Fe_{cyt} \tag{10}$$

The *IRT1*-mRNA (variable *IRT1*) is considered to be synthesized at a constant rate (k_3) and degraded by a first-order process with respect to *IRT1*. The IRT1-transporter (variable IRT1) synthesis rate is proportional to the amount of *IRT1* transcript (variable *IRT1*). IRT1-protein is considered to be removed in an iron-dependent manner, where iron binds and thereby activates the IRT1-degrading enzyme E_{set}. The fraction of activated enzyme removing IRT1 is given as f_a^{Fe}:

$$f_a^{Fe} = \frac{Fe_{cyt}}{K_a^{Fe} + Fe_{cyt}} \tag{11}$$

where K_a^{Fe} is the dissociation constant between Fe_{cyt} and the nonactive form of the
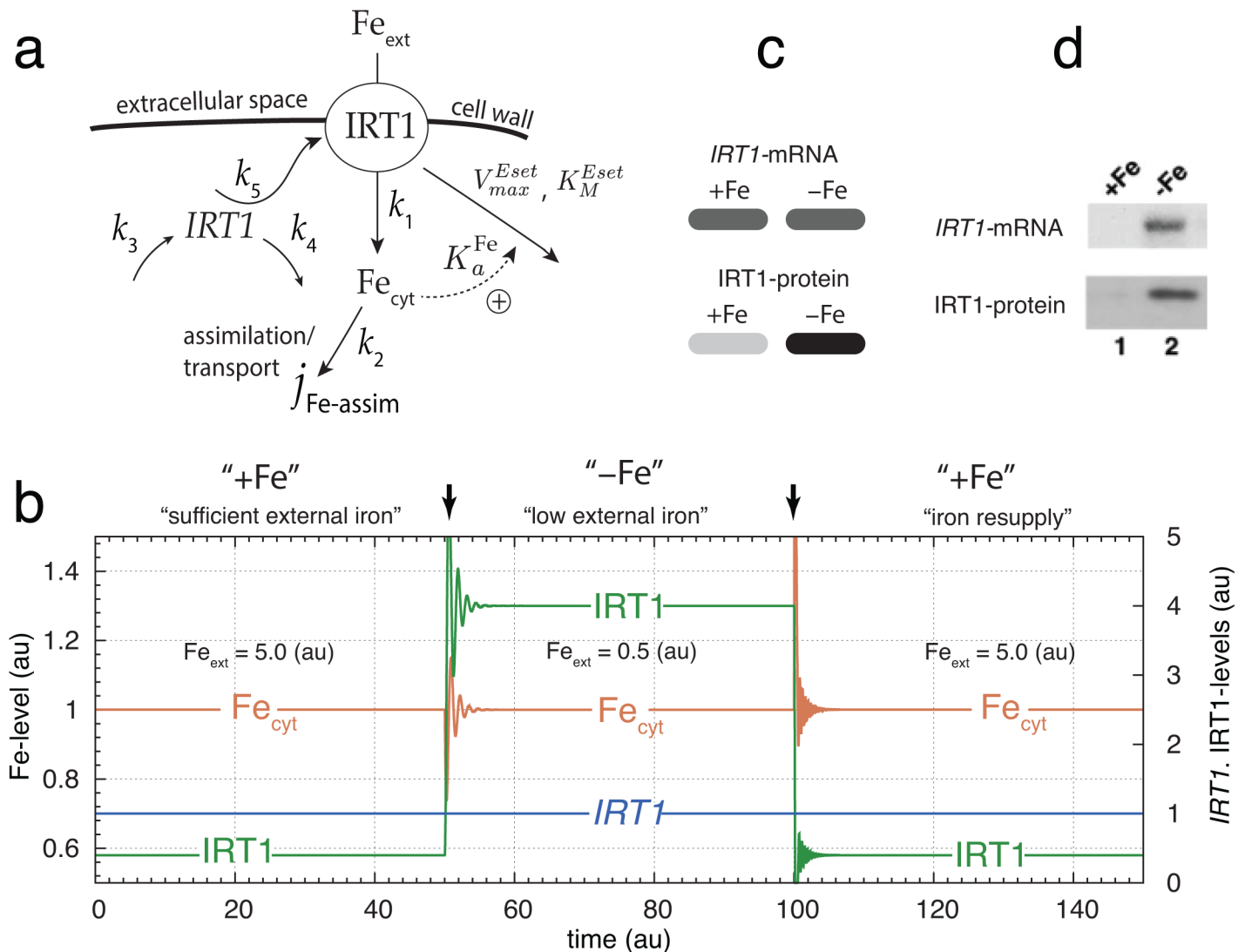
Fig 3. Regulatory loop of high affinity iron uptake and cytosolic iron homeostasis based on an iron-dependent IRT1 degradation. (a) Scheme of the control loop. Fe_{ext} and Fe_{cyt} denote external and cytosolic iron, respectively. *IRT1* and IRT1 denote mRNA and its protein, respectively. The extracellular iron concentration, Fe_{ext}, is allowed to change to different but constant levels. (b) Homeostasis in cytosolic iron levels (Fe_{cyt}) with respect to sufficient and low external iron. The set-point for the level of cytosolic iron is given by Eq (12) and is arbitrarily set to $Fe_{cyt}^{set} = 1.0$. In the first phase (time $t = 0$ to $t = 50$) $Fe_{ext} = 5.0$ and relative high. To keep iron at its homeostatic set-point during this phase the required concentration of IRT1 is relative low. In the second phase starting at $t = 50$ (arrow) Fe_{ext} is reduced to 0.5. Due to this reduction the IRT1 level is increased to keep the cytosolic iron concentration close at its set-point. In the third phase ($t = 100$ to $t = 150$) iron is resupplied and IRT1 levels decrease again. Other rate parameters remain unchanged during the three phases, i.e. $k_1 = 1.0$, $k_2 = 2.0$, $k_3 = 1.0 \times 10^2$, $k_4 = 1.0 \times 10^2$, $k_5 = 1.0 \times 10^2$, $V_{max}^{Eset} = 2.0 \times 10^2$, $K_M^{Eset} = 1.0 \times 10^{-4}$, and $K_a^{Fe} = 1.0$. Initial concentrations are $Fe_{cyt,0} = 1.0$, $IRT1_{0 = 1.0}$, and $IRT1_{0 = 0.4}$. (c) Representation of results in a 'blot-like' manner. +Fe and –Fe denote sufficient and low external ion conditions, respectively. For each component (*IRT1*, IRT1) the gray levels (0–100%) reflect the relative *IRT1*/IRT1 concentrations at +Fe and –Fe conditions. (d) Experimental data, slightly rearranged from Fig 6A in Ref. [21].

doi:10.1371/journal.pone.0147120.g003

IRT1-degrading enzyme not having bound IRT1. The binding event between iron and the IRT1-removing enzyme can be seen as part of an iron sensing mechanism, where the amount of IRT1 reflects the concentration of cytosolic iron and may mediate this information to the regulation of other substances. Such a mechanism appears to be present to nitrate uptake in Arabidopsis where the nitrate transporters influences other uptake mechanisms [43, 44]. Due to the binding of iron to E_{set}, f_a^{Fe} has saturation properties. IRT1-degradation by the activated enzyme is described by a Michaelis-Menten type of reaction with a relative strong binding to its substrate, i.e. with a relative low $K_M^{E_{set}}$ value. Experiments indicate that IRT1 is degraded by the proteasome after ubiquinitation [23, 45]. The kinetics of the iron-induced IRT1 removal defines the set-point for cytosolic iron homeostasis. Setting both $IRT1 = 0$ and $\dot{IRT1} = 0$ together with $K_M^{E_{set}} \ll$ IRT1, gives the following expression for the set-point (see S2 Text):

$$\mathrm{Fe}_{cyt,set} = \frac{k_3 \cdot k_5 \cdot K_a^{Fe}}{k_4 \cdot V_{max}^{E_{set}} - k_3 \cdot k_5} \tag{12}$$

The condition $K_M^{E_{set}} \ll$ IRT1 represents an idealization used here for illustration, such that the controlled variable (here cytosolic iron) is kept at its set-point with high precision. However, it is presently not known at what degree of precision biochemical controllers usually operate. For controllers where $K_M^{E_{set}}$ values do not meet the condition $K_M^{E_{set}} \ll$ IRT1 it has been shown that the value of $K_M^{E_{set}}$ is a direct measure of the controller's accuracy [37].

Fig 3b shows the levels of Fe_{cyt}, *IRT1*-mRNA and the IRT1 transporter for sufficient ("+Fe") and low ("−Fe") external iron conditions. The term 'sufficent' here means that the level of external iron is such that no significant up-regulation of IRT1 is necessary to meet the iron need of the cell/plant as expressed by the assimilation flux $j_{Fe\text{-}assim} = k_2 \cdot \mathrm{Fe}_{cyt}$. In the case when the external iron concentration is low IRT1 needs up-regulation in order to meet the plant's requirement for iron while keeping Fe_{cyt} close to its set-point.

Fig 3c shows the *IRT1* transcript and IRT1 protein levels in terms of a blot/gel-like view as would be obtained by Northern and Western blots, respectively. The relative concentrations in IRT1 at +Fe and −Fe conditions are expressed in terms of the gray percentage value, where the high IRT1 value of 4.0 (at "−Fe" condition) has been assigned a gray-level of 100% (black), while at the +Fe condition the gray-level has been reduced to 10% in accordance with the reduction of the IRT1-level to 0.4.

Ignoring for the moment the *IRT1* transcript data, the IRT1 protein dynamics of the controller are in good qualitative agreement with experimental results [10, 21, 23, 45], showing that at sufficient iron conditions, IRT1 levels are kept low but increase when iron becomes less available (Fig 3b and 3c). Fig 3d shows corresponding experimental data by Connolly et al. [21]. The up-regulation of *IRT1*-mRNA and IRT1-protein at iron-deficient conditions is clearly seen. When iron is resupplied, experiments and calculations show that IRT1-levels decrease again (see Fig 2 in [21] and Fig 3b).

IRT1 Overexpression Leads to Saturation in Iron Signaling

When *IRT1* is over-expressed in plants with an *IRT1*-knockout background Barberon et al. [23] observed accumulation of IRT1, metal/iron overload, and oxidative stress. Under these conditions IRT1 degradation rates were found to be independent of the amount of supplied external iron, in contrast to the suggestion of an iron-dependent degradation of IRT1 considered in earlier work [21, 22]. We here show that under *IRT1* overexpression conditions the observation of iron overload and an iron-independent degradation of IRT1 can be rationalized by the homeostasis model in Fig 3a. In the model overexpression of *IRT1* is achieved by

increasing k_3. As k_3 increases the set-point of cytosolic iron also increases see Eq (12) and leads to elevated levels of cytosolic iron, which can explain the observation [23] of iron overload. Fig 4a shows the model's behavior when k_3 is increased from 1.0×10^2 to 1.9×10^2 at $t = 50$. This increase in k_3 leads to an increased set-point from 1.0 to 19.0. In addition, IRT1 levels are also increased in order to maintain homeostasis at the higher set-point. Although the homeostatic performance of the system is still functional at the new k_3 value, the signaling pathway from iron to IRT1 degradation is reaching its capacity limit with a change of f_a^{Fe} from 0.50 to 0.95. Accordingly, the rate of IRT1 degradation, $j_{IRT1-degr}$, described by Eq (13) has moved close to its maximum level of $V_{max}^{E_{set}}$ (Fig 4a).

$$j_{IRT1-degr} = \frac{Fe_{cyt}}{K_a^{Fe} + Fe_{cyt}} \cdot \frac{V_{max}^{E_{set}} \cdot IRT1}{K_M^{E_{set}} + IRT1} \qquad (13)$$

Once the synthesis rate of IRT1 ($j_{IRT1-synth} = k_5 \cdot IRT1$) exceeds the capacity $V_{max}^{E_{set}}$ of the IRT1-degrading enzyme, IRT1-protein and cytosolic iron levels increase dramatically. This is shown in the third phase of Fig 4a when $k_3 = 1 \times 10^3$. As a result of the large $j_{IRT1-synth}$ flux, the signaling pathway from iron to IRT1 degradation becomes saturated, i.e., $f_a^{Fe} \to 1$, the negative feedback is no longer operational, and IRT1 levels rise. At this stage the IRT1 degradation rate becomes saturated and independent of the external iron concentration, as illustrated in Fig 4b. In Fig 4c the calculated overexpression results are replotted in form of dot blots. Fig 4d shows corresponding experimental results taken from Fig 1D by Barberon et al. [23]. In agreement with the modeling results for IRT1-protein (Fig 3c), the experimental results by Barberon et al. show the same wild-type (WT) regulation as previously observed by Connolly et al. [21] (Fig 3d) and others. However, for 35S-IRT1 overexpression conditions, the results by Barberon et al. [23] indicate a loss of IRT1-regulation by external iron (Fig 4d), while Fig 6B (lanes 1 and 2) by Connolly et al. [21] still shows such a regulation. This apparent disagreement between the 35S-IRT1 overexpression results can be rationalized by assuming that the IRT1 synthesis rate in the experiments by Connolly et al. rate is still below the capacity of the cell's IRT1 degradation capacity, while for the IRT1 overexpression conditions by Barberon et al. the IRT1 synthesis rate has exceeded that capacity. The signaling event from cytosolic iron to the degradation machinery for IRT1 in Fig 3a can be interpreted to be part of the system's iron sensing mechanism which breaks down. The breakdown/saturation of a still undiscovered iron sensing mechanism would be another alternative to interpret the iron-insensitivity of IRT1 degradation/inactivation at strong IRT1 overexpressing conditions. Thus, overexpression studies alone do not provide sufficient evidence to rule out an iron-dependent degradation/inactivation of IRT1 at normal operating conditions.

Model including *IRT1*-mRNA and regulation by *FIT*

The model in Fig 3a did not include the regulation of *IRT1* transcript levels as indicated by the experiments shown in Fig 3d. In addition, the *FIT* gene was found to be essential for the high-affinity uptake of iron [10, 12, 21, 23, 46, 47]. The complex between AtbHLH38/AtbHLH39 and FIT has been found to activate *IRT1* and *FRO2* expression [13]. In addition, FIT was found to take part in the inhibiting of IRT1-protein degradation [12]. Model calculations shown below predict that the FIT-induced inhibition of IRT1 degradation has a role in improving (decreasing) the response time of the plant's iron homeostatic system.

Fig 5a shows an extended model for the high-affinity uptake of iron and cytosolic iron homeostasis including *IRT1* and *FIT* transcript and protein levels. The rate equations of this model are given in S3 Text. The variable TF (Fig 5a) lumps together the transcription factors
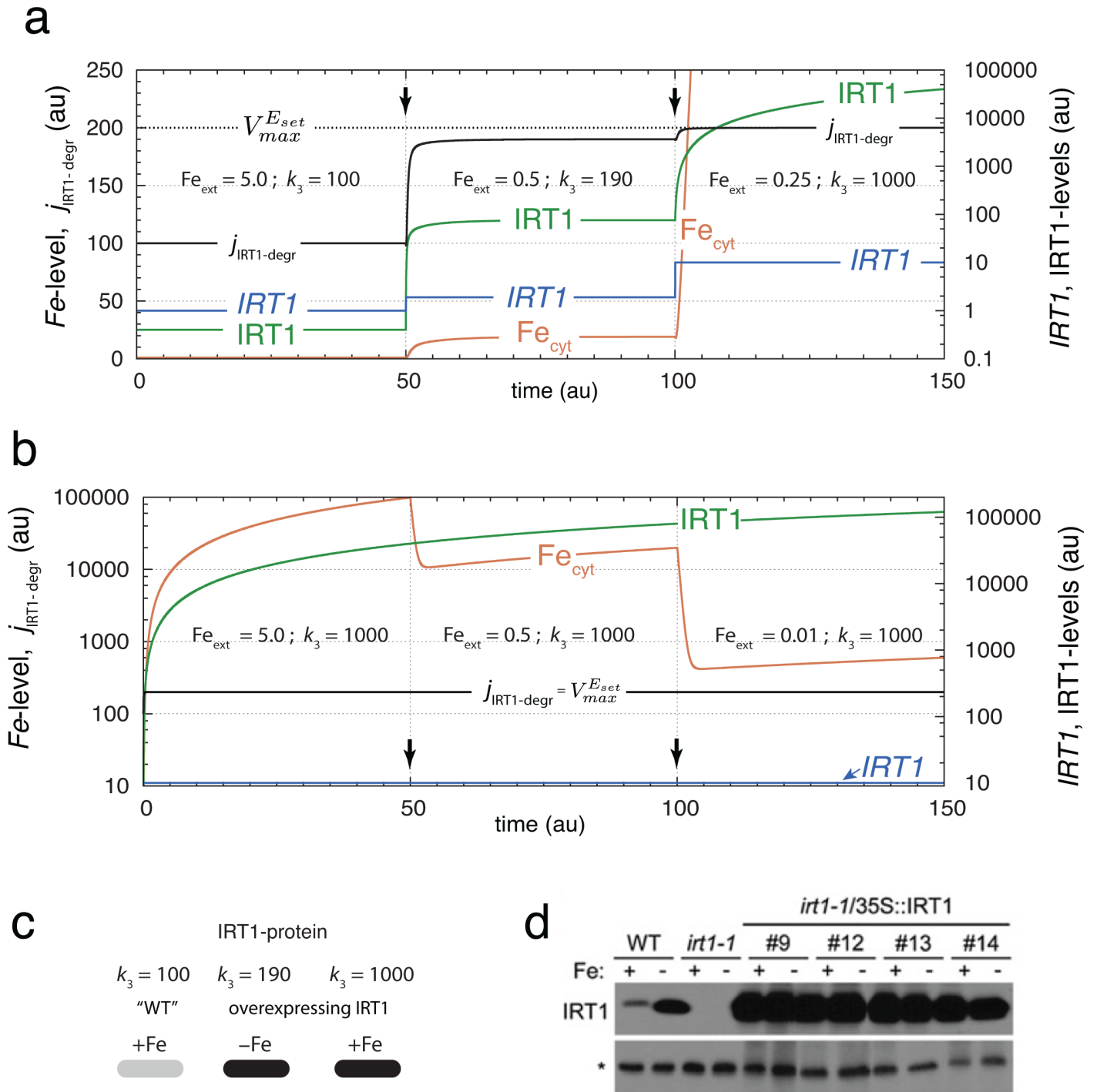
Fig 4. *IRT1* overexpression leads to an increased iron set-point, iron overload and to saturation in the iron-dependent degradation of IRT1. (a) Increase of *IRT1* synthesis rate k_3 at different external iron levels. At times $t = 50$ and $t = 100$ (indicated by arrows) the values of Fe_{ext} and k_3 are changed as indicated in the figure. As long as the IRT1 syntesis rate $j_{IRT1-synth}$ is lower than its degradation rate ($t = 0$ to $t = 100$), the cytosolic iron concentration is under homeostatic control at its new set-point Eq (12). When $j_{IRT1-synth}$ becomes larger than $j_{IRT1-degr}$ iron levels rise and the IRT1 degradation rate $j_{IRT1-degr}$ goes into saturation ($t = 100$ to $t = 150$). The negative feedback loop is broken and iron homeostasis lost. (b) Demonstration of iron-independent degradation of IRT1 when $j_{IRT1-synth} > j_{IRT1-degr}$. The overexpression rate (k_3) is kept constant at 1×10^3 while external iron concentrations Fe_{ext} are changing. For each Fe_{ext} value (5.0, 0.5, and 0.01) the IRT1 degradation rate is at its maximum value $V_{max}^{E_{set}}$ and independent of the cytosolic iron concentration. Rate constants, except k_3, are as in Fig 3c. (c) Calculated IRT1 expression levels shown as "dot-blots". (d) Corresponding experimental results by Barberon et al. (Fig 1D in [23]).

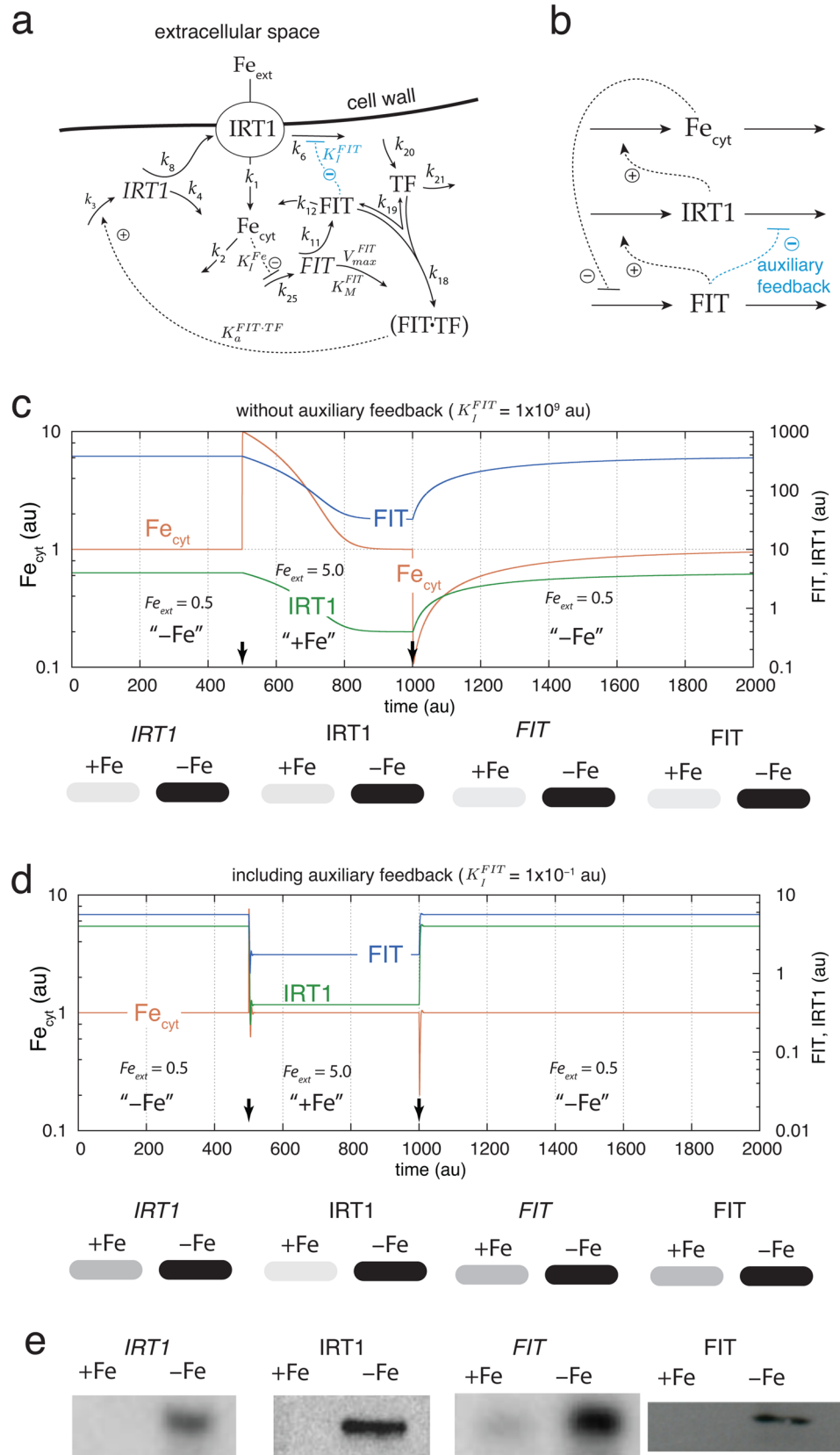doi:10.1371/journal.pone.0147120.g004

Fig 5. Model for iron uptake including *IRT1* and *FIT*. (a) Reaction scheme of the model. See S3 Text for rate equations. (b) Overview over the feedback structure of the model at the protein and cytosolic iron levels. The inhibition outlined in blue defines an additional auxiliary negative feedback which does not influence the set-point of cytosolic iron, but accelerates the adaptation kinetics of the controller (see (d)). (c) Regulation of *IRT1*- and *FIT*-mRNA and protein levels and response kinetics of the iron uptake system at low (-Fe) and high (+Fe) external iron concentrations and in the absence of the auxiliary feedback ($K_I^{FIT} = 1 \times 10^9$). The lower part of the panel shows the *IRT1*- and *FIT*-mRNA and protein levels in a blot-like representation, where high levels under -Fe conditions have a gray scale of 100%, while +Fe levels have a reduced gray scale in relation to their reduced numerical values. (d) Same as in (c), but now in the presence of the auxiliary feedback ($K_I^{FIT} = 1 \times 10^{-1}$). Note the improvement in the adaptation kinetics of the system. Rate constants for (c) and (d): $k_1 = 1.0$, $k_2 = 2.0$, $k_3 = 1 \times 10^2$, $k_4 = 1.0$, $k_6 = 4 \times 10^2$, $k_8 = 1 \times 10^2$, $K_I^{FIT} = 1 \times 10^9$, $k_{11} = 1 \times 10^3$, $k_{12} = 1 \times 10^3$, $K_a^{FIT \cdot TF} = 1 \times 10^4$, $k_{18} = 1 \times 10^2$, $k_{19} = 1 \times 10^1$, $k_{20} = 1 \times 10^4$, $k_{21} = 2 \times 10^4$, $K_I^{Fe} = 1.0$, $k_{25} = 4.0$, $V_{max}^{FIT} = 2.0$, $K_M^{FIT} = 1 \times 10^{-4}$. Initial concentrations for (c): $Fe_{cyt0} = 1.0$, $IRT1_0 = 4.0$, $IRT1_0 = 16.0$, $FIT_0 = 381.0$, $TF_0 = 0.5$, $FIT \cdot TF_{0 = 1905.0}$, $FIT_0 = 381.0$. Initial concentrations for (d): $Fe_{cyt0} = 1.0$, $IRT1_0 = 4.0$, $IRT1_0 = 0.3$, $FIT_0 = 5.6$, $TF_0 = 0.5$, $FIT \cdot TF_{0 = 28.0}$, $FIT_0 = 5.6$. (e) Experimental results of IRT1 and FIT mRNA and protein levels in wild-type Arabidopsis roots under iron sufficient ("+Fe") and iron deficient ("-Fe") conditions. The IRT1-protein and mRNA results as well as the *FIT*-mRNA blot are reproduced with permission from Fig 1 of Ref. [12]. The FIT-protein Western blot is reproduced with permission from Fig 4A of Ref. [47].

doi:10.1371/journal.pone.0147120.g005

AtbHLH38 and AtbHLH39 which bind to FIT (FIT·TF) and activate the transcription of *IRT1* [13]. The activations of *FRO2* and AHA2/7 by FIT is not considered in the model. Many experiments confirm that the levels of *IRT1*- and *FIT*-mRNAs as well as IRT1 and FIT proteins are up- or down-regulated when external iron levels are decreased or increased, respectively. [10, 21, 23, 45–47]. The simplest way to rationalize the behaviors of these components is to place the homeostatic regulation point of cytosolic iron at the level of *FIT*-mRNA. An increase of *FIT*-mRNA levels when external and cytosolic iron are low (iron limiting conditions) will induce an increase in FIT-protein, and as a follow-up reaction, an increase in both *IRT1*-mRNA and IRT1 protein levels. Thus, separate regulatory loops for *IRT1*-mRNAs as well as FIT and IRT1-protein levels are in principle not necessary, although additional regulations are possible such as the identified FIT-induced inhibition of IRT1-degradation [12], which increase the performance of the homeostatic system. In the model, the regulation of *FIT*-mRNA is included in form of an iron-induced inhibition of *FIT*-mRNA synthesis. Alternatively, an iron-induced activation of *FIT*-mRNA degradation is possible, which shows practically the same up- and down-regulation characteristics of the components (data not shown). These are the only two possibilities of inflow controller motifs which match with the up- and down-regulation of the "E"-component [37] in the regulatory loop (here the "E"-component is the *FIT*-mRNA). There are presently no experimental indications favoring the inhibition of *FIT*-mRNA synthesis over an activation of its degradation or *vice versa*. For this model (Fig 5a) the set-point for cytosolic iron is determined by the rate equation for *FIT*:

$$\dot{FIT} = \frac{k_{25} \cdot K_I^{Fe}}{K_I^{Fe} + Fe_{cyt}} - \frac{V_{max}^{FIT} \cdot FIT}{K_M^{FIT} + FIT} \tag{14}$$

Setting $\dot{FIT} = 0$ and using the condition/assumption that $K_M^{FIT} \ll FIT$ the following expression for the set-point of Fe_{cyt} is obtained

$$Fe_{cyt,set}^{FIT} = K_I^{Fe} \left(\frac{k_{25}}{V_{max}^{FIT}} - 1 \right) \tag{15}$$

Fig 5b shows the outline of the feedback structures for the model in panel a. The inhibition of IRT1 degradation induced by FIT, outlined in blue, defines an additional experimentally
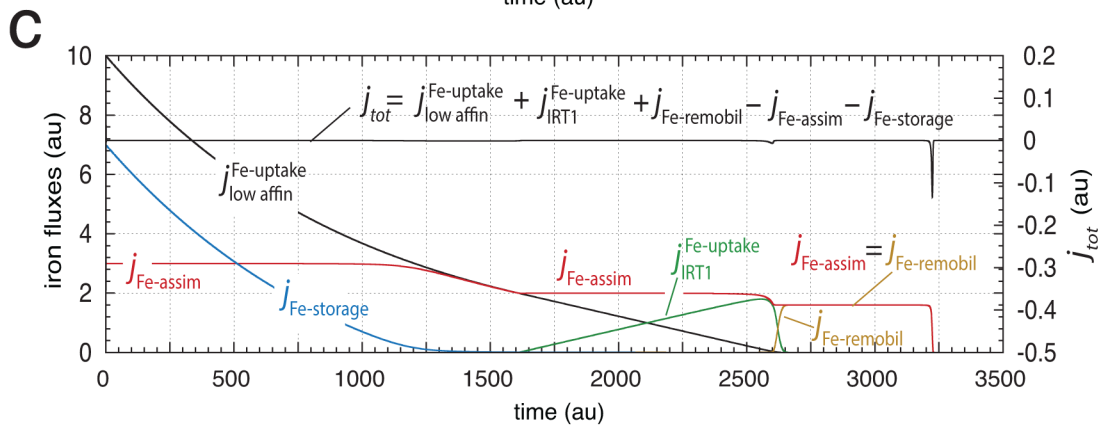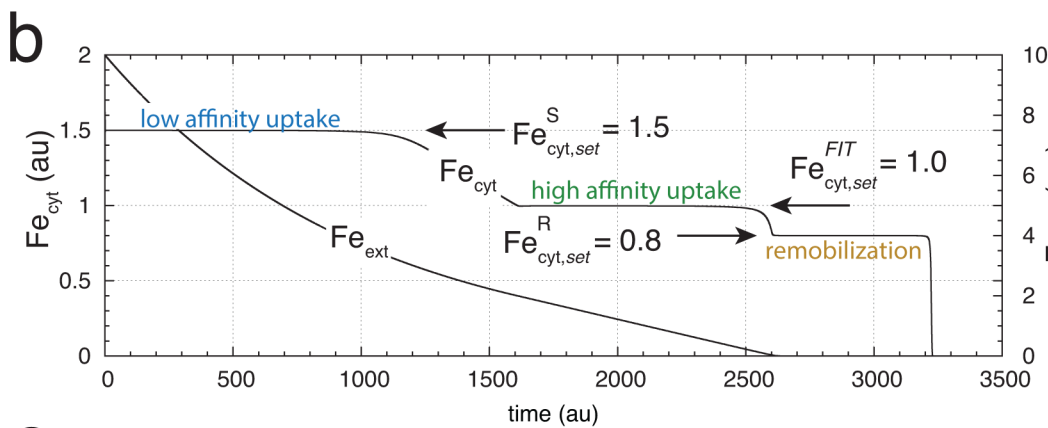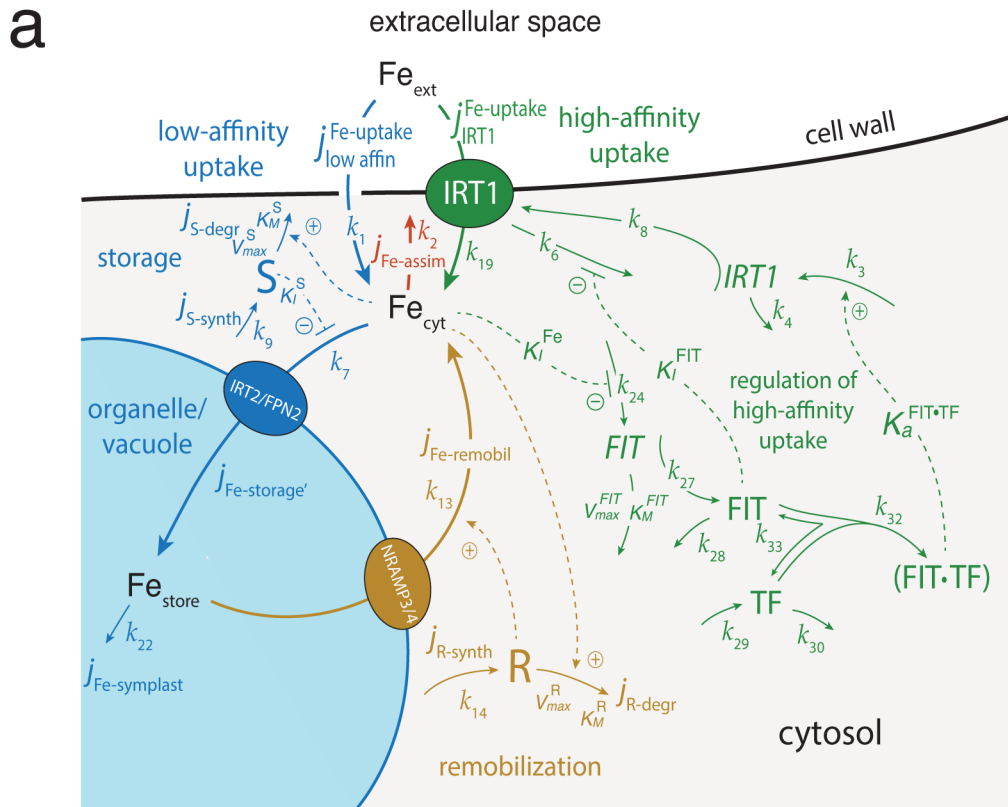
Fig 6. Model of plant iron homeostasis integrating uptake, storage, assimilation/transport and remobilization from the store. (a) The model combines a low-affinity iron uptake based on an iron-dependent derepression mechanism of inhibitor S [53], which leads to iron storage (outlined in blue), an R-based iron remobilization mechanism from the store (outlined in ochre), the FIT-based high-affinity iron uptake mechanism from Fig 5a (outlined in green) and a lumped expression for the iron assimilation and transport flux to other parts of the plant (outlined in red). Note the renumbering for some of the rate constants in comparison with Fig 5a. See S4 Text for rate equations. (b) Calculation showing cytosolic and external iron concentrations during the low- and high-affinity uptake of iron and iron remobilization from the vacuole. (c) Same calculation as in (b), but showing the different iron fluxes. Rate constants and initial concentrations for (b) and (c): $k_1 = 1.0$, $k_2 = 2.0$, $k_3 = 1 \times 10^2$, $k_4 = 1.0$, $k_6 = 4 \times 10^2$, $k_7 = 1 \times 10^2$, $k_8 = 1 \times 10^2$, $k_9 = 15.0$, $V_{max}^S = 10.0$, $K_M^S = 1 \times 10^{-4}$, $K_I^S = 0.1$, $k_{13} = 0.5$, $k_{14} = 0.8$, $V_{max}^R = 1.0$, $K_M^R = 1 \times 10^{-6}$, $k_{19} = 0.5$, $k_{22} = 5 \times 10^{-4}$, $K_I^{Fe} = 1.0$, $k_{24} = 4.0$, $V_{max}^{FIT} = 2.0$, $K_M^{FIT} = 1 \times 10^{-4}$, $k_{27} = 1 \times 10^3$, $k_{28} = 1 \times 10^3$, $k_{29} = 1 \times 10^4$; $k_{30} = 2 \times 10^4$, $k_{32} = 1 \times 10^2$, $k_{33} = 10.0$, $K_a^{FIT \cdot TF} = 1 \times 10^4$, $K_I^{FIT} = 0.01$. $Fe_{ext,0} = 10.0$, all other initial concentrations are zero.

doi:10.1371/journal.pone.0147120.g006

identified negative feedback [12]. We incorporated this feedback, like that in Fig 2d, without an integral controller and with no influence upon the set-point value of Fe_{cyt} Eq (15).

Although having no influence on Fe_{cyt}'s set-point, the feedback generated by the FIT-induced inhibition of IRT1 degradation, significantly improves the controller's adaptation kinetics to the set-point (Fig 5c and 5d) and indicates a biological role for the FIT-induced inhibition of IRT1 degradation. We suggest to call this type of negative feedback loop for an 'auxiliary feedback'.

Besides the inhibition of IRT1 degradation by FIT [12] several other additional negative feedback arrangements either in form of auxiliary feedbacks or containing an integral controller appear possible. An additional candidate for a helper feedback may be an iron-dependent degradation of FIT. Experiments have shown that the proteasomal degradation of FIT is necessary for the plant's iron deficiency response [47, 48], but whether cytosolic iron regulates a proteasomal FIT degradation is presently not known. Also an iron-dependent degradation of IRT1 as previously suggested [21] can act as an additional auxiliary feedback.

The model results described in Fig 5c and 5d are in good agreement with corresponding experimental findings shown in Fig 5e where the results from different laboratories are shown, i.e., the respective up- and down-regulations of IRT1 and FIT transcript and protein levels at high and low external iron conditions.

Iron Homeostasis Including Storage and Remobilization

At high external iron concentrations iron is taken up by an IRT1-independent mechanism [10], possibly due to a low-affinity uptake of iron by other metal-ion transporters [49–51].

Under high cytosolic iron concentrations the inflow controller in Fig 5a will automatically shut-down [37], while iron can still enter the cell and lead to high and potentially toxic iron levels [52]. To avoid the buildup of excess iron in the cytosol plants store and bind inflowing iron. One of the components is ferritin, a protein which is able to bind a large number of iron atoms. Ferritin is found in leaf chloroplasts [53] but also in mitochondria [54] probably reflecting the high abundance of iron in these organelles. Although ferritins are essential to protect the cell and its organelles from oxidative stress, ferritin is not considered to be a major iron pool for either seedling development or for the photosynthetic apparatus [52, 55]. Another molecule, Nicotianamine (NA), which is synthesized from three S-adenosylmethionine molecules, binds both Fe(II) and Fe(III). Although the binding constants are high for both oxidation states, Fe(II) is kinetically stabilized under aerobic conditions [14]. The NA-Fe(II) complex appears to be an important intracellular iron transport form for all plants and is a relative poor Fenton reagent [14, 16–18]. In the tomato mutant plant *chloronerva* where NA is nonfunctional due to a single base change [15], retarded growth of shoots and roots was observed, despite the fact

that sufficient external iron was made available. In these plants precipitation of Fe(III)-phosphate occurred [56], providing an explanation why iron in *chloronerva* appeared less available.

Localization studies of NA, used as an indicator for the NA-Fe(II) complex and thereby for iron, revealed for different wild type plants that at low external iron concentrations most of the NA label appeared in the cytosol. For high iron loading conditions NA was found to be located in the vacuole [16]. This suggests that the vacuole acts as an iron store at sufficient high external iron concentrations, but that no vacuolar storage of iron occurs under iron-limiting conditions. In yeast, iron is stored as Fe(III), which during its remobilization from the vacuole is reduced by Fre6p to Fe(III) [57]. For plants, no corresponding metalloreductase has so far been found [58] indicating that the main storage form of iron in the vacuole appears to be complexed Fe(II).

A candidate for transporting iron into the vacuole is IRT2, a homolog to IRT1 which is co-regulated with FRO2 and IRT1 [59]. IRT2 is expressed in intracellular membranes. It has been suggested that IRT2 is part of an overflow mechanism [18], which sequesters iron into the vacuole or other non-characterized intracellular vesicles [60]. Other candidate transporters for moving cytosolic iron into the vacuole are VIT1 (during seed development) [61], FPN2 [62], a homolog of mammalian ferroportin and VTL [63]. In Arabidopsis, NRAMP3 and NRAMP4 take part in the iron remobilization from the vacuole into the cytosol during iron deficiency [18, 64, 65].

Fig 6a shows a model integrating low- and high-affinity iron uptake with iron storage and iron remobilization. The S4 Text describes the rate equations. The change in cytosolic iron concentration can be expressed by the following fluxes

$$\dot{\text{Fe}}_{\text{cyt}} = j_{\text{low affin}}^{\text{Fe-uptake}} + j_{\text{IRT1}}^{\text{Fe-uptake}} - j_{\text{Fe-assim}} - j_{\text{Fe-storage}} + j_{\text{Fe-remobil}} \qquad (16)$$

$j_{\text{low affin}}^{\text{Fe-uptake}}$ (outlined in blue) is the low affinity uptake rate of iron, which we for the sake of simplicity assumed to be proportional to the concentration of the external iron concentration Fe_{ext}, i.e., not necessarily only diffusion-driven

$$j_{\text{low affin}}^{\text{Fe-uptake}} = k_1 \cdot \text{Fe}_{\text{ext}} \qquad (17)$$

$j_{\text{IRT1}}^{\text{Fe-uptake}}$ (outlined in green) is the high affinity uptake rate of iron

$$j_{\text{IRT1}}^{\text{Fe-uptake}} = k_{19} \cdot \text{IRT1} \cdot \text{Fe}_{\text{ext}} \qquad (18)$$

where IRT1 is the concentration of IRT1-protein in the membrane.

$j_{\text{Fe-assim}}$ (outlined in red) is the flux combining the assimilation of iron and its transport to other parts of the plant. This flux is described as Eq (10), i.e.

$$j_{\text{Fe-assim}} = k_2 \cdot \text{Fe}_{\text{cyt}} \qquad (19)$$

$j_{\text{Fe-storage}}$ (outlined in blue) is the flux moving cytosolic iron into the store (the vacuole and other organelles). The activation of this flux is based on a mechanism which was described for the activation of ferritins in the presence of excess iron [53]. Under low iron conditions the transport of iron into the store is blocked by a still unknown inhibitor S. However, when iron inflow into the cytoplasm becomes high S is degraded by the proteosome in an iron-dependent manner and iron can enter the store [53]. The iron flux into the store is described by

$$j_{\text{Fe-storage}} = k_7 \cdot \text{Fe}_{\text{cyt}} \cdot \left(\frac{K_I^S}{K_I^S + \text{S}} \right) \qquad (20)$$

where K_I^S is a inhibition constant by which S inhibits $j_{\text{Fe-storage}}$. For the sake of simplicity the

concentration of the transporters (IRT2/FPN2) moving iron into the store are considered to be constant, i.e., $k_7 = k_7' \cdot (\text{IRT2/FPN2}) = $ constant, such that the flux of iron into the store is proportional to the concentration of Fe_{cyt}. The inhibitor S may act at different levels, i.e. either directly inhibiting the transporter which moves iron into the store, or, like in the case of ferritin, acting at the transcriptional level [53].

The remobilization of iron from the store into the cytosol (ochre-colored) is formulated as

$$j_{\text{Fe-remobil}} = k_{13} \cdot \text{Fe}_{\text{store}} \cdot \text{R} \tag{21}$$

where R is the remobilization regulator and an inflow controller with respect to cytosolic iron. The rate equation of R is given as:

$$\dot{\text{R}} = j_{\text{R-synth}} - j_{\text{R-degr}} = k_{14} - \left(\frac{V_{max}^{\text{R}} \cdot \text{R}}{K_M^{\text{R}} + \text{R}} \right) \cdot \text{Fe}_{\text{cyt}} \tag{22}$$

Also here the concentration of the transporters NRAMP3/4 is considered to be constant, i.e., $k_{13} = k_{13}' \cdot \text{NRAMP3/4} = $ constant. We are not aware of any identified feedback scheme with respect to iron remobilization from the vacuole. In this respect, the here suggested mechanism involving R is hypothetical. The set-point concentration of cytosolic iron with respect to inflow controller R is obtained by setting Eq (22) to zero and assuming that $K_M^{\text{R}} \ll \text{R}$. Solving for Fe_{cyt} gives

$$\text{Fe}_{\text{cyt,set}}^{\text{R}} = \frac{k_{14}}{V_{max}^{\text{R}}} \tag{23}$$

The kinetics of the external iron source is described as

$$\dot{\text{Fe}}_{\text{ext}} = -j_{\text{low affin}}^{\text{Fe-uptake}} - j_{\text{IRT1}}^{\text{Fe-uptake}} \tag{24}$$

The rate equation for iron within the store is given by

$$\dot{\text{Fe}}_{\text{store}} = j_{\text{Fe-storage}} - j_{\text{Fe-remobil}} - j_{\text{Fe-symplast}} \tag{25}$$

Finally, we have the rate equation of the regulator S for iron storage:

$$\dot{\text{S}} = j_{\text{S-synth}} - j_{\text{S-degr}} \tag{26}$$

where $j_{\text{S-synth}}$ is a constant (k_9), while $j_{\text{S-degr}}$ is activated by cytosolic iron and described by Michaelis-Menten kinetics

$$j_{\text{S-degr}} = \text{Fe}_{\text{cyt}} \left(\frac{V_{max}^{\text{S}} \cdot \text{S}}{K_M^{\text{S}} + \text{S}} \right) \tag{27}$$

The set-point during storage is determined by setting $\dot{\text{S}} = 0$ Eq (26), which leads to

$$\text{Fe}_{\text{cyt,set}}^{\text{S}} = \frac{j_{\text{S-synth}}}{V_{max}^{\text{S}}} \tag{28}$$

To ensure that the combined controllers work flawlessly together, their set-points need to be in a certain hierarchical order as wind-up may occur otherwise [36, 37]. We have chosen the rate parameters such that $\text{Fe}_{\text{cyt,set}}^{\text{S}} = 1.5$, $\text{Fe}_{\text{cyt,set}}^{FIT} = 1.0$, and $\text{Fe}_{\text{cyt,set}}^{\text{R}} = 0.8$. The different set-point values also allow that the phases of storage, high-affinity uptake, and remobilization from the store can be easily identified (Fig 6b).

Fig 6b shows the concerted and integrative behavior of the combined controllers. The initial concentration of external iron, Fe_{ext}, is 10.0 and relative high. At this condition the IRT1-based

high-affinity uptake system is down-regulated and a still unknown uptake system moves iron into the cell [10]. To avoid a buildup of toxic iron within the cytosol, the excess of incoming iron (relative to the set-point of the S-controller) is moved by the S-controller into the vacuole/ store. The negative feedback control loop for keeping homeostasis during storage (controller motif 6, [37]) is analogous to the motif identified for ferritin regulation ([53], see also above).

The flux into the store, $j_{\text{Fe-storage}}$, decreases gradually with the decrease in the external iron concentration. At approximately 1250 time units (Fig 6b and 6c) there is not sufficient external ion available to maintain the homeostasis by the S-controller and the cytosolic iron concentration decreases (Fig 6b). As $j_{\text{low affin}}^{\text{Fe-uptake}}$ decreases the need for iron is satisfied by an increased IRT1-based uptake flux, $j_{\text{IRT1}}^{\text{Fe-uptake}}$, such that $j_{\text{low affin}}^{\text{Fe-uptake}}$ and $j_{\text{IRT1}}^{\text{Fe-uptake}}$ together compensate the assimilatory flux $j_{\text{Fe-assim}}$ and maintain cytosolic iron homeostasis, i.e.,

$$j_{\text{Fe-assim}} = j_{\text{low affin}}^{\text{Fe-uptake}} + j_{\text{IRT1}}^{\text{Fe-uptake}} \tag{29}$$

The successive up-regulation of $j_{\text{IRT1}}^{\text{Fe-uptake}}$ continues until the external supply of iron is exhausted. In the model calculation this occurs at about 2600 time units (Fig 6b and 6c). In the final phase starting at about 2600 time units, the remobilization flux $j_{\text{Fe-remobil}}$ from the store is activated and solely balances the assimilatory flux $j_{\text{Fe-assim}}$.

The arrangement of controller motifs in Fig 6a leads only to iron storage when a large amount of iron can enter the cell. In case the external iron concentration is low and iron becomes limiting, no significant storage of iron can occur. This is illustrated in Fig 7 showing the system's response when the external iron concentration is kept at 1.0. While the FIT/IRT1--based controller balances the assimilatory flux $j_{\text{Fe-assim}}$ no significant flux into the store occurs, and the store is emptied by the putative symplast iron transport [66, 67] which connects the vacuole to other parts of the plant (described by the flux $j_{\text{Fe-symplast}} = k_{22} \cdot \text{Fe}_{\text{store}}$, Fig 6a). This strategy of vacuolar iron storage when there is only a surplus of external iron available fits well with experimental findings when NA-labelled plants are exposed to low and high external iron concentrations [16].

Increasing Vacuolar Storage of Iron at Low External Iron Concentrations

According to the World Health Organization iron deficiency is the most common and widespread nutritional disorder in the world [68]. As reviewed by Jeong and Guerinot [6] an understanding of iron homeostasis is not only important for getting better plant growth and increasing crop yields but also to improve human nutrition. Different approaches for iron biofortification in plants have been used, among them increasing the amount of ferritin and NA. Based on the properties of the here described controller motifs, we suggest a model-guided approach to increase the amount of stored iron in roots even when iron is taken up by the high-affinity system. The strategy is to place an inflow controller with respect to vacuolar iron within the vacuolar membrane while target the controller molecule into the vacuole (Fig 8a, outlined in gray). An inflow controller motif will try to maintain an iron homeostatic set-point in the vacuole defined by the negative feedback structure of the controller molecule I. Four controller motifs are in principle possible to achieve inflow control [37]. We here illustrate the approach using motif 1 [37] with an iron-induced degradation of controller I, while I is activating the inflow of iron into the vacuole (Fig 8a). The set-point of this controller is given by the ratio between I expression and its maximum degradation rate. An expression for the set-point is obtained by setting the rate equation for I to zero and solving for Fe_{store}, i.e.,

$$\dot{\text{I}} = k_{18} - \text{Fe}_{\text{store}} \cdot \left(\frac{V_{max}^{\text{I}} \cdot \text{I}}{K_M^{\text{I}} + \text{I}} \right) = 0 \tag{30}$$
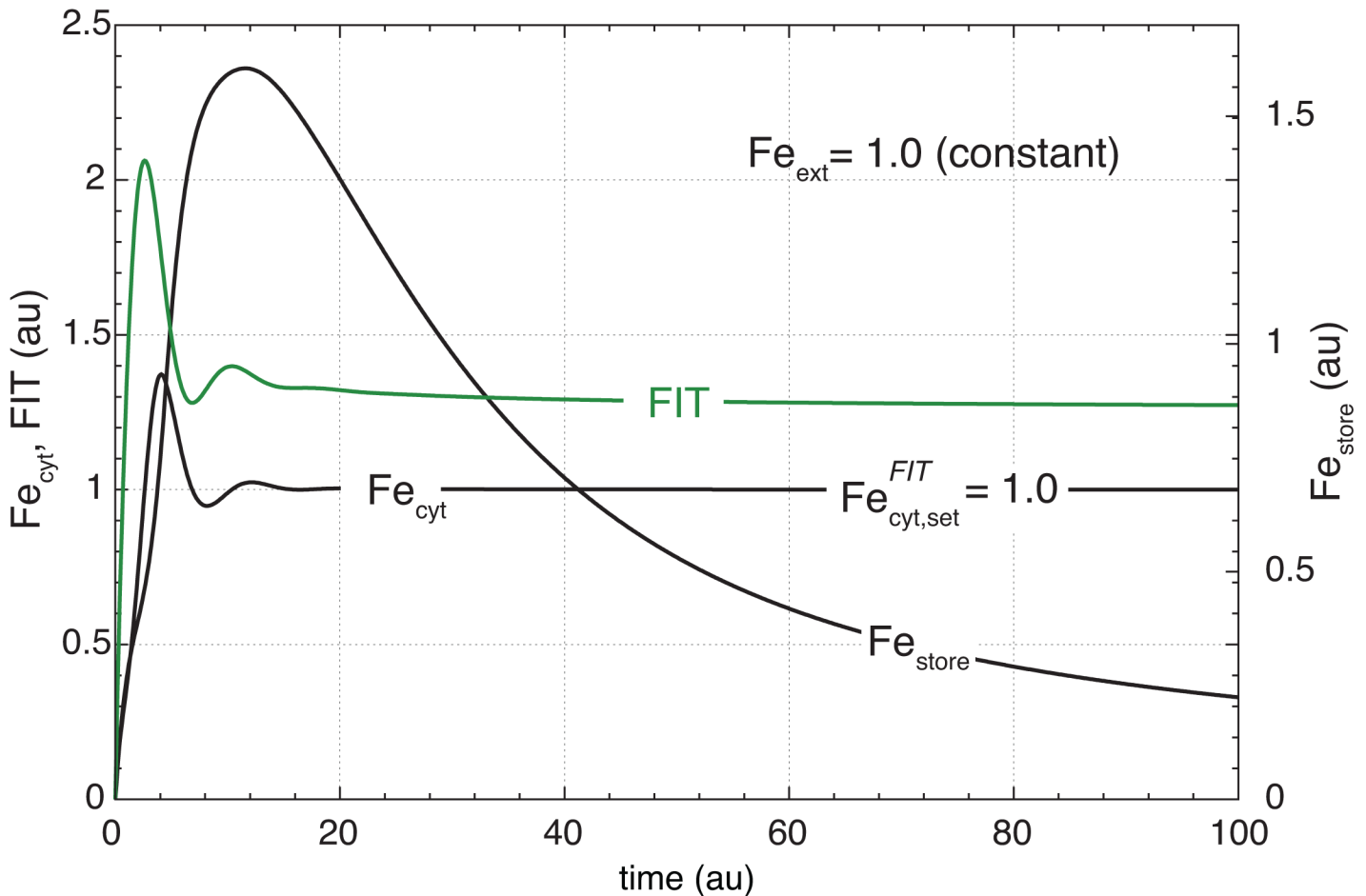
Fig 7. Iron-based derepression mechanism of iron storage is not active at low external iron concentrations. The figure shows that the iron-based derepression mechanism for iron storage (Fig 6a) cannot activate iron storage at low external iron concentrations when the IRT1 high-affinity uptake system is active. In this calculation the external iron concentration Fe$_{ext}$ is kept constant at 1.0. Initial concentrations and rate constants for this calculation are as in Fig 6b and 6c, except for k_{22} (= 0.1) which accounts for a symplastic removal of iron out of the vacuole and leads to a decrease in Fe$_{store}$. The FIT and IRT1-based high affinity uptake is able to keep the cytosolic iron at its set-point Fe$_{cyt,set}^{FIT}$ = 1.0, while the S-based outflow controller (Fig 6a), responsible for iron storage, is inactive.

doi:10.1371/journal.pone.0147120.g007

Assuming that $K_M^I \ll I$, the vacuolar iron set-point is given by

$$\text{Fe}_{store,set}^I = \frac{k_{18}}{V_{max}^I} \qquad (31)$$

Fig 8b illustrates the behavior of the system with a Fe$_{store,set}^I = 700$. Even at low iron conditions the system now accumulates iron in the vacuole, where Fe$_{store,set}^I$ is an upper limit for the vacuolar iron concentration. At present this approach is purely theoretical, but transport routes to incorporate newly synthesized/overexpressed transporters such as FRP2 into the vacuolar membrane are known and can be used in a synthetic biology approach to generate iron accumulating plants. The usage of the vacuole to store increased amounts of iron has the advantage that increased iron concentration inside the vacuole are nontoxic to the plant, because FRP2-mediated transport of iron protects the plant from iron shock [69]. Although there has
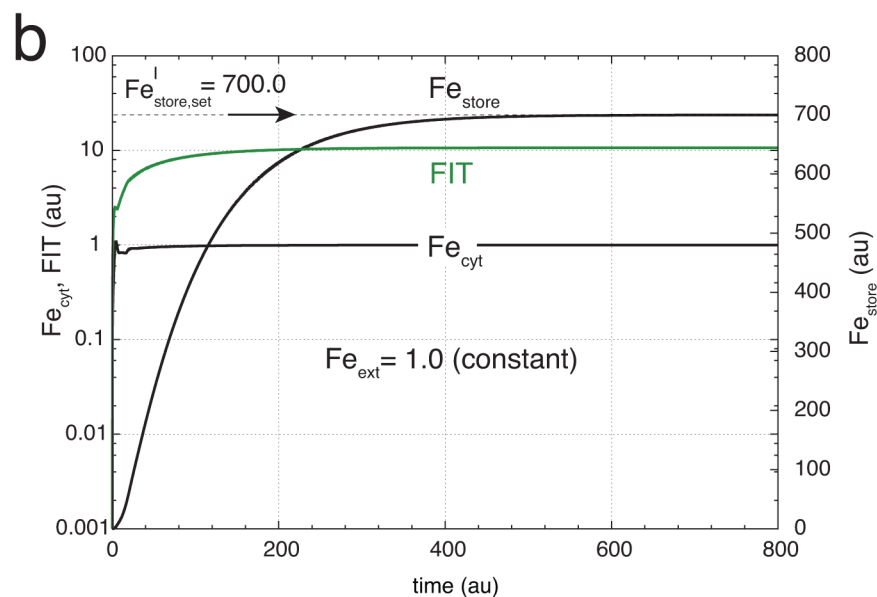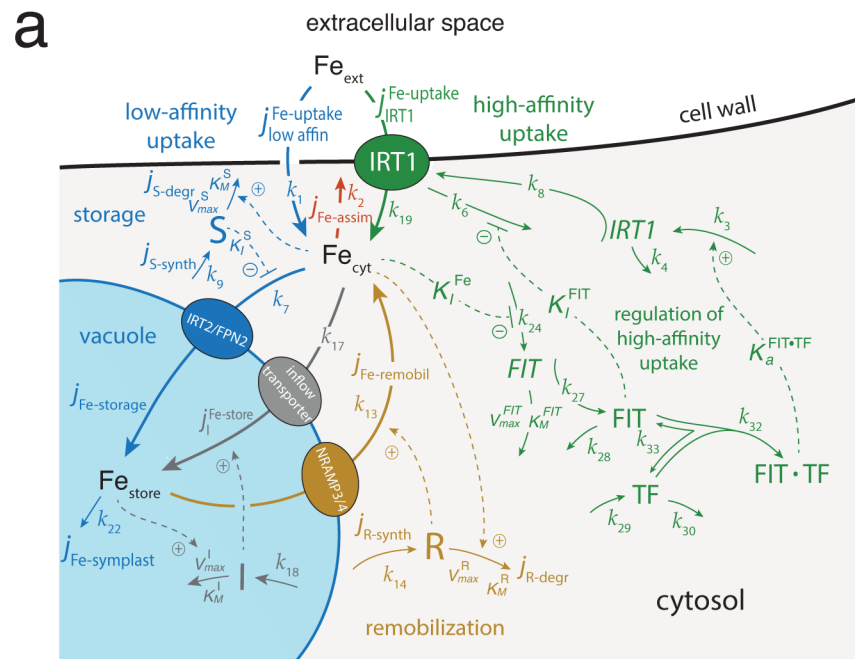
Fig 8. Iron storage during high-affinity uptake. (a) The model is an extension of that in Fig 6a containing in addition inflow controller molecule I inside the vacuole which activates a transporter located in the vacuolar membrane. Controller molecule I is subject to an iron-dependent degradation. The rate equation for I is: $\dot{I} = k_{18} - Fe_{store} \cdot V_{max}^{I} \cdot I/(K_M^{I} + I)$ (b) Calculation showing the increase of iron in the vacuole, Fe_{store}, as a function of time. The iron set-point inside the vacuole is given by Eq (31) and set to 700.0. The flux of iron entering the vacuole due to controller I is given as: $j_I^{Fe-store} = k_{17} \cdot Fe_{cyt} \cdot I$. The additional parameter values are: $k_{17} = 1 \times 10^{-3}$, $k_{18} = 700.0$, $V_{max}^{I} = 1.0$, $K_M^{I} = 1 \times 10^{-4}$. Other parameter values and initial concentrations as in Fig 6. The initial concentration of controller I is zero.

doi:10.1371/journal.pone.0147120.g008

been made considerable progress in the understanding of plant iron regulation, our knowledge about the iron regulatory elements, their concentrations and kinetics are still fragmentary. We hope that the here suggested model-guided approach may stimulate further theoretical and experimental work leading to an increased understanding and better modification of iron regulation in higher plants.

Hierarchical Arrangement of Inflow and Outflow Controllers

We have presented a model of plant iron homeostasis in root cells with emphasis on non-gramineaceous plants/Arabidopsis, which integrates low- and high-affinity iron uptake, iron storage and remobilization as well iron assimilation and transport of iron to other parts of the plant. The model is based on a hierarchical arrangement of set-points when combining inflow and outflow controllers with respect to cytosolic iron. The outflow control arrangement (controller S) has the highest set-point ($Fe_{cyt,set}^{S}$) and moves iron from the cytoplasm to another part of the cell (store). An inflow controller associated with a high-affinity uptake system provides the next level of control with a set-point ($Fe_{cyt,set}^{FIT}$) below that of the outflow controller. This control level does not allow for storage, but balances the need of the cell for iron to maintain its functions while keeping the cytosolic iron concentration at a high enough level. The final level of control is that of remobilizing iron from the store back into the cytosol to balance the assimilatory flux and the need to maintain cellular function. The set-point of this control level ($Fe_{cyt,set}^{R}$) has the lowest value. This hierarchical arrangement of set-points

$$Fe_{cyt,set}^{S} > Fe_{cyt,set}^{FIT} > Fe_{cyt,set}^{R} \qquad (32)$$

allows for a concerted and cooperative manner of how the controllers are activated in response to external and internal iron supplies and requirements. Otherwise, if for example $Fe_{cyt,set}^{FIT} <$ $Fe_{cyt,set}^{R}$ the store of iron would be always emptied *before* external iron is used by the high affinity uptake system. When $Fe_{cyt,set}^{S} < Fe_{cyt,set}^{FIT}$ the iron concentration will settle somewhere between both set-points, while both controllers are actively trying to move the cytosolic iron concentration to the level of their respective set-points. This behavior, when both S- and FIT-controllers are working "against each other" and leading to a constant upregulation of S, *FIT*-mRNA, and FIT-protein is referred to as "integral wind-up" [37]. To avoid windup, we anticipate that in all robustly homeostatic controlled systems a hierarchy of set-points is established as described by Eq (32) in order to maintain a concerted operation of the individual controllers.

Sensor Mechanisms

Organisms need certain mechanisms to adapt to environmental changes. In this respect sensors and sensor mechanisms appear necessary to get information about the environment. The sequence of processes

$$\text{sensing} \rightarrow \text{transduction} \rightarrow \text{reaction} \qquad (33)$$

has been considered as a general model how organisms and cells adapt to a changing environment [70]. In the literature [6] the anticipation of a not yet identified iron sensor upstream of *FIT* participating in iron homeostasis has been expressed. The regulatory structure in Fig 5b for the uptake of iron suggests an iron-sensing and signaling mechanism from Fe_{cyt} to *FIT*. As indicated above two possibilities exists for an inflow controller arrangement which matches the FIT and IRT1 dynamics upon external iron changes: either an inhibition of *FIT*-mRNA synthesis or an activation of its degradation. In addition to these sensing mechanisms as part of the regulatory negative feedback, there may be additional sensors that could, for example, be part

of a feedforward control mechanism [71] to further optimize the system's homeostatic response. In feedforward control environmental changes are measured/sensed and integrated into the negative feedback loop. Feedforward behavior is preset and appears to have developed due to an evolutionary process. Feedforward mechanisms are associated with anticipative behaviors of a system [72, 73] as found for example in circadian control [74, 75]. Plant iron has actually been found to be under a circadian regulation [53, 76]. Although not considered here, we have recently found that some of the controller motifs can be extended to work under oscillatory conditions [40], which will be a subject of further investigations.

Supporting Information

S1 Table. Overview of Determined Root and Leaf Iron Concentrations (*µg* Fe per mg dry weight of tissue).
(PDF)

S1 Text. Robustness of Integral Control.
(PDF)

S2 Text. Dynamic model of Fig 3 and Derivation of Eq (12).
(PDF)

S3 Text. Dynamic model of Fig 5.
(PDF)

S4 Text. Dynamic model of Fig 6.
(PDF)

S5 Text. How to run the matlab files.
(TXT)

S1 File. matlab_fig2c.m file.
(M)

S2 File. ODEs_for_Figure_2c.m file.
(M)

S3 File. matlab_fig2d.m file.
(M)

S4 File. ODEs_for_Figure_2d.m file.
(M)

S5 File. matlab_fig3b.m file.
(M)

S6 File. ODEs_for_Figure_3b.m file.
(M)

S7 File. matlab_fig4a.m file.
(M)

S8 File. matlab_fig4b.m file.
(M)

S9 File. ODEs_for_Figure_4ab.m file.
(M)

S10 File. matlab_fig5c.m file.
(M)

S11 File. matlab_fig5d.m file.
(M)

S12 File. ODEs_for_Figure_5cd.m file.
(M)

S13 File. matlab_fig6.m file.
(M)

S14 File. ODEs_for_Figure_6bc.m file.
(M)

S15 File. matlab_fig7.m file.
(M)

S16 File. ODEs_for_Figure_7.m file.
(M)

S17 File. matlab_fig8b.m file.
(M)

S18 File. ODEs_for_Figure_8b.m file.
(M)

Acknowledgments

Author Contributions

Conceived and designed the experiments: XMX TD PR. Performed the experiments: OA CHS KT XMX TD PR. Analyzed the data: OA CHS KT XMX TD PR. Contributed reagents/materials/analysis tools: OA CHS TD PR. Wrote the paper: TD PR.

References

1. Römheld V, Marschner H. Evidence for a specific uptake system for iron phytosiderophores in roots of grasses. Plant Physiology. 1986; 80(1):175–180. doi: 10.1104/pp.80.1.175 PMID: 16664577

2. Curie C, Briat JF. Iron transport and signaling in plants. Annu Rev Plant Biol. 2003; 54:183–206. doi: 10.1146/annurev.arplant.54.031902.135018 PMID: 14509968

3. Briat JF, Curie C, Gaymard F. Iron utilization and metabolism in plants. Current Opinion in Plant Biology. 2007; 10:276–282. doi: 10.1016/j.pbi.2007.04.003 PMID: 17434791

4. Kim SA, Guerinot ML. Mining iron: iron uptake and transport in plants. FEBS Letters. 2007; 581 (12):2273–2280. doi: 10.1016/j.febslet.2007.04.043 PMID: 17485078

5. Walker EL, Connolly EL. Time to pump iron: iron-deficiency-signaling mechanisms of higher plants. Current Opinion in Plant Biology. 2008; 11:530–535. doi: 10.1016/j.pbi.2008.06.013 PMID: 18722804

6. Jeong J, Guerinot ML. Homing in on iron homeostasis in plants. Trends in Plant Science. 2009; 14 (5):280–285. doi: 10.1016/j.tplants.2009.02.006 PMID: 19375375

7. Kobayashi T, Nishizawa NK. Iron uptake, translocation, and regulation in higher plants. Annual review of plant biology. 2012; 63:131–52. doi: 10.1146/annurev-arplant-042811-105522 PMID: 22404471

8. Eide D, Broderius M, Fett J, Guerinot ML. A novel iron-regulated metal transporter from plants identified by functional expression in yeast. PNAS. 1996; 93(11):5624–5628. doi: 10.1073/pnas.93.11.5624 PMID: 8643627

9. Korshunova YO, Eide D, Clark WG, Guerinot ML, Pakrasi HB. The IRT1 protein from Arabidopsis thaliana is a metal transporter with a broad substrate range. Plant Molecular Biology. 1999; 40(1):37–44. doi: 10.1023/A:1026438615520 PMID: 10394943

10. Vert G, Grotz N, Dédaldéchamp F, Gaymard F, Guerinot ML, Briat JF, et al. IRT1, an Arabidopsis transporter essential for iron uptake from the soil and for plant growth. The Plant Cell. 2002; 14(6):1223–1233. doi: 10.1105/tpc.001388 PMID: 12084823

11. Bauer P, Ling HQ, Guerinot ML. FIT, the FER-LIKE IRON DEFICIENCY INDUCED TRANSCRIPTION FACTOR in Arabidopsis. Plant Physiology and Biochemistry. 2007; 45(5):260–261. doi: 10.1016/j.plaphy.2007.03.006 PMID: 17466530

12. Colangelo EP, Guerinot ML. The essential basic helix-loop-helix protein FIT1 is required for the iron deficiency response. The Plant Cell. 2004; 16(12):3400–3412. doi: 10.1105/tpc.104.024315 PMID: 15539473

13. Yuan Y, Wu H, Wang N, Li J, Zhao W, Du J, et al. FIT interacts with AtbHLH38 and AtbHLH39 in regulating iron uptake gene expression for iron homeostasis in Arabidopsis. Cell Research. 2008; 18(3):385–397. doi: 10.1038/cr.2008.26 PMID: 18268542

14. von Wirén N, Klair S, Bansal S, Briat JF, Khodr H, Shioiri T, et al. Nicotianamine chelates both FeIII and FeII. Implications for metal transport in plants. Plant Physiology. 1999; 119(3):1107–1114. doi: 10.1104/pp.119.3.1107 PMID: 10069850

15. Ling HQ, Koch G, Bäumlein H, Ganal MW. Map-based cloning of chloronerva, a gene involved in iron uptake of higher plants encoding nicotianamine synthase. PNAS. 1999; 96(12):7098–7103. doi: 10.1073/pnas.96.12.7098 PMID: 10359845

16. Pich A, Manteuffel R, Hillmer S, Scholz G, Schmidt W. Fe homeostasis in plant cells: does nicotianamine play multiple roles in the regulation of cytoplasmic Fe concentration? Planta. 2001; 213(6):967–976. doi: 10.1007/s004250100573 PMID: 11722133

17. Hell R, Stephan UW. Iron uptake, trafficking and homeostasis in plants. Planta. 2003; 216(4):541–551. PMID: 12569395

18. Schmidt W. Iron stress responses in roots of strategy I plants. In: Barton LL, Abadia J, editors. Iron Nutrition in Plants and Rhizospheric Microorganisms. Dordrecht: Springer; 2006. pp. 229–250.

19. Rellán-Álvarez R, Abadía J, Álvarez-Fernández A. Formation of metal-nicotianamine complexes as affected by pH, ligand exchange with citrate and metal exchange. A study by electrospray ionization time-of-flight mass spectrometry. Rapid Communications in Mass Spectrometry. 2008; 22(10):1553–1562. doi: 10.1002/rcm.3523 PMID: 18421700

20. Gitan RS, Eide DJ. Zinc-regulated ubiquitin conjugation signals endocytosis of the yeast ZRT1 zinc transporter. Biochem J. 2000; 346:329–336. doi: 10.1042/bj3460329 PMID: 10677350

21. Connolly EL, Fett JP, Guerinot ML. Expression of the IRT1 metal transporter is controlled by metals at the levels of transcript and protein accumulation. The Plant Cell. 2002; 14(6):1347–1357. doi: 10.1105/tpc.001263 PMID: 12084831

22. Kerkeb L, Mukherjee I, Chatterjee I, Lahner B, Salt DE, Connolly EL. Iron-induced turnover of the Arabidopsis IRON-REGULATED TRANSPORTER1 metal transporter requires lysine residues. Plant Physiology. 2008; 146(4):1964–1973. doi: 10.1104/pp.107.113282 PMID: 18305211

23. Barberon M, Zelazny E, Robert S, Conéjéro G, Curie C, Friml J, et al. Monoubiquitin-dependent endocytosis of the iron-regulated transporter 1 (IRT1) transporter controls iron uptake in plants. PNAS. 2011; 108(32):E450–E458. doi: 10.1073/pnas.1100659108 PMID: 21628566

24. Cannon W. Organization for Physiological Homeostasis. Physiol Rev. 1929; 9:399–431.

25. Hughes GM. Homeostasis and Feedback Mechanisms. New York: Academic Press; 1964.

26. Langley, LL, editor. Homeostasis. Origins of the Concept. Stroudsbourg, Pennsylvania: Dowden, Hutchinson & Ross, Inc.; 1973.

27. Schulkin J. Allostasis, Homeostasis and the Costs of Physiological Adaptation. Cambridge, Massachusetts: Cambridge University Press; 2004.

28. Wilkie J, Johnson M, Reza K. Control Engineering. An Introductory Course. New York: Palgrave; 2002.

29. Yi TM, Huang Y, Simon MI, Doyle J. Robust perfect adaptation in bacterial chemotaxis through integral feedback control. PNAS. 2000; 97(9):4649–53. doi: 10.1073/pnas.97.9.4649 PMID: 10781070

30. El-Samad H, Goff JP, Khammash M. Calcium homeostasis and parturient hypocalcemia: an integral feedback perspective. J Theor Biol. 2002; 214:17–29. doi: 10.1006/jtbi.2001.2422 PMID: 11786029

31. Ingalls BP, Yi TM, Iglesias PA. Using Control Theory to Study Biology. In: Szallasi Z and Stelling J and Periwal V, editor. System Modeling in Cellular Biology. Cambridge, Massachusetts: MIT Press; 2006. p. 243–267.

32. Cloutier M, Wellstead P. The control systems structures of energy metabolism. Journal of The Royal Society Interface. 2009;

33. Ni XY, Drengstig T, Ruoff P. The control of the controller: Molecular mechanisms for robust perfect adaptation and temperature compensation. Biophys J. 2009; 97:1244–1253. doi: 10.1016/j.bpj.2009.06.030 PMID: 19720012

34. Ang J, Bagh S, Ingalls BP, McMillen DR. Considerations for using integral feedback control to construct a perfectly adapting synthetic gene network. J Theor Biol. 2010 Oct; 266(4):723–738. doi: 10.1016/j.jtbi.2010.07.034 PMID: 20688080

35. Jolma IW, Ni XY, Rensing L, Ruoff P. Harmonic oscillations in homeostatic controllers: Dynamics of the p53 regulatory system. Biophys J. 2010; 98(5):743–52. doi: 10.1016/j.bpj.2009.11.013 PMID: 20197027

36. Huang Y, Drengstig T, Ruoff P. Integrating fluctuating nitrate uptake and assimilation to robust homeostasis. Plant, Cell and Environment. 2011; 35:917–928. doi: 10.1111/j.1365-3040.2011.02462.x PMID: 22070777

37. Drengstig T, Jolma I, Ni X, Thorsen K, Xu X, Ruoff P. A basic set of homeostatic controller motifs. Biophys J. 2012; 103(9):2000–2010. doi: 10.1016/j.bpj.2012.09.033 PMID: 23199928

38. Drengstig T, Ni X, Thorsen K, Jolma I, Ruoff P. Robust adaptation and homeostasis by autocatalysis. The Journal of Physical Chemistry B. 2012; 116(18):5355–5363. doi: 10.1021/jp3004568 PMID: 22506960

39. Ang J, McMillen DR. Physical Constraints on Biological Integral Control Design for Homeostasis and Sensory Adaptation. Biophys J. 2013 Jan; 104(2):505–515. doi: 10.1016/j.bpj.2012.12.015 PMID: 23442873

40. Thorsen K, Agafonov O, Selstø CH, Jolma IW, Ni XY, Drengstig T, et al. Robust Concentration and Frequency Control in Oscillatory Homeostats. PLOS ONE. 2014; 9(9):e107766. doi: 10.1371/journal.pone.0107766 PMID: 25238410

41. Radhakrishnan K, Hindmarsh AC. Description and Use of LSODE, the Livermore Solver for Ordinary Differential Equations. NASA Reference Publication 1327, Lawrence Livermore National Laboratory Report UCRL-ID-113855. Cleveland, OH 44135-3191: National Aeronautics and Space Administration, Lewis Research Center; 1993.

42. Grossoehme NE, Akilesh S, Guerinot ML, Wilcox DE. Metal-Binding Thermodynamics of the Histidine-Rich Sequence from the Metal-Transport Protein IRT1 of *Arabidopsis thaliana*. Inorganic Chemistry. 2006; 45(21):8500–8508. doi: 10.1021/ic0606431 PMID: 17029360

43. Krouk G, Lacombe B, Bielach A, Perrine-Walker F, Malinska K, Mounier E, et al. Nitrate-regulated auxin transport by NRT1. 1 defines a mechanism for nutrient sensing in plants. Developmental Cell. 2010; 18(6):927–937. doi: 10.1016/j.devcel.2010.05.008 PMID: 20627075

44. Wang YY, Hsu PK, Tsay YF. Uptake, allocation and signaling of nitrate. Trends in Plant Science. 2012; 17(8):458–467. doi: 10.1016/j.tplants.2012.04.006 PMID: 22658680

45. Shin LJ, Lo JC, Chen GH, Callis J, Fu H, Yeh KC. IRT1 DEGRADATION FACTOR1, a RING E3 ubiquitin ligase, regulates the degradation of IRON-REGULATED TRANSPORTER1 in Arabidopsis. The Plant Cell. 2013; 25(8):3039–3051. doi: 10.1105/tpc.113.115212 PMID: 23995086

46. Lingam S, Mohrbacher J, Brumbarova T, Potuschak T, Fink-Straube C, Blondet E, et al. Interaction between the bHLH transcription factor FIT and ETHYLENE INSENSITIVE3/ETHYLENE INSENSITIVE3-LIKE1 reveals molecular linkage between the regulation of iron acquisition and ethylene signaling in Arabidopsis. The Plant Cell. 2011; 23(5):1815–1829. doi: 10.1105/tpc.111.084715 PMID: 21586684

47. Meiser J, Lingam S, Bauer P. Posttranslational regulation of the iron deficiency basic helix-loop-helix transcription factor FIT is affected by iron and nitric oxide. Plant Physiology. 2011; 157(4):2154–2166. doi: 10.1104/pp.111.183285 PMID: 21972265

48. Sivitz A, Grinvalds C, Barberon M, Curie C, Vert G. Proteasome-mediated turnover of the transcriptional activator FIT is required for plant iron-deficiency responses. The Plant Journal. 2011; 66(6):1044–1052. doi: 10.1111/j.1365-313X.2011.04565.x PMID: 21426424

49. Eide DJ. The molecular biology of metal ion transport in Saccharomyces cerevisiae. Annual Review of Nutrition. 1998; 18(1):441–469. doi: 10.1146/annurev.nutr.18.1.441 PMID: 9706232

50. Guerinot ML. The ZIP family of metal transporters. Biochimica et Biophysica Acta (BBA)-Biomembranes. 2000; 1465(1):190–198. doi: 10.1016/S0005-2736(00)00138-3

51. Wintz H, Fox T, Wu YY, Feng V, Chen W, Chang HS, et al. Expression profiles of Arabidopsis thaliana in mineral deficiencies reveal novel transporters involved in metal homeostasis. Journal of Biological Chemistry. 2003; 278(48):47644–47653. doi: 10.1074/jbc.M309338200 PMID: 13129917

52. Ravet K, Touraine B, Boucherez J, Briat JF, Gaymard F, Cellier F. Ferritins control interaction between iron homeostasis and oxidative stress in Arabidopsis. The Plant Journal. 2009; 57(3):400–412. doi: 10.1111/j.1365-313X.2008.03698.x PMID: 18826427

53. Briat JF, Duc C, Ravet K, Gaymard F. Ferritins and iron storage in plants. Biochimica et Biophysica Acta (BBA)-General Subjects. 2010; 1800(8):806–814. doi: 10.1016/j.bbagen.2009.12.003

54. Vigani G, Tarantino D, Murgia I. Mitochondrial ferritin is a functional iron-storage protein in cucumber (Cucumis sativus) roots. Frontiers in Plant Science. 2013; 4:316. doi: 10.3389/fpls.2013.00316 PMID: 23967005

55. Taiz L, Zeiger E. Plant Physiology. Sunderland, MA: Sinauer Associates; 2010.

56. Becker R, Fritz E, Manteuffel R. Subcellular localization and characterization of excessive iron in the nicotianamine-less tomato mutant chloronerva. Plant Physiology. 1995; 108(1):269–275. PMID: 12228472

57. Singh A, Kaur N, Kosman DJ. The metalloreductase Fre6p in Fe-efflux from the yeast vacuole. Journal of Biological Chemistry. 2007; 282(39):28619–28626. doi: 10.1074/jbc.M703398200 PMID: 17681937

58. Jain A, Wilson GT, Connolly EL. The diverse roles of FRO family metalloreductases in iron and copper homeostasis. Frontiers in Plant Science. 2014; 5:100. doi: 10.3389/fpls.2014.00100 PMID: 24711810

59. Vert G, Barberon M, Zelazny E, Séguéla M, Briat JF, Curie C. Arabidopsis IRT2 cooperates with the high-affinity iron uptake system to maintain iron homeostasis in root epidermal cells. Planta. 2009; 229 (6):1171–1179. doi: 10.1007/s00425-009-0904-8 PMID: 19252923

60. Thomine S, Vert G. Iron transport in plants: better be safe than sorry. Current Opinion in Plant Biology. 2013; 16(3):322–327. doi: 10.1016/j.pbi.2013.01.003 PMID: 23415557

61. Kim SA, Punshon T, Lanzirotti A, Li L, Alonso JM, Ecker JR, et al. Localization of iron in Arabidopsis seed requires the vacuolar membrane transporter VIT1. Science. 2006; 314(5803):1295–1298.

62. Morrissey J, Baxter IR, Lee J, Li L, Lahner B, Grotz N, et al. The ferroportin metal efflux proteins function in iron and cobalt homeostasis in Arabidopsis. The Plant Cell. 2009; 21(10):3326–3338. doi: 10.1105/tpc.109.069401 PMID: 19861554

63. Gollhofer J, Timofeev R, Lan P, Schmidt W, Buckhout TJ. Vacuolar-Iron-Transporter1-Like Proteins Mediate Iron Homeostasis in Arabidopsis. PLOS ONE. 2014; 9(10):e110468. doi: 10.1371/journal.pone.0110468 PMID: 25360591

64. Curie C, Alonso J, Le Jean M, Ecker J, Briat J. Involvement of NRAMP1 from Arabidopsis thaliana in iron transport. Biochem J. 2000; 347:749–755. doi: 10.1042/0264-6021:3470749 PMID: 10769179

65. Jaquinod M, Villiers F, Kieffer-Jaquinod S, Hugouvieux V, Bruley C, Garin J, et al. A proteomics dissection of Arabidopsis thaliana vacuoles isolated from cell culture. Molecular & Cellular Proteomics. 2007; 6(3):394–412. doi: 10.1074/mcp.M600250-MCP200

66. Velikanov GA. Vacuolar symplast and methodological approach to monitoring water self-diffusion between vacuoles of contacting root cells. Russian Journal of Plant Physiology. 2007 Sep; 54(5):683–692. doi: 10.1134/S1021443707050172

67. Andreev IM. The vacuolar symplast: Does it really exist in plants? (Comments on Publications of G.A. Velikanov et al. in Russian Journal of Plant Physiology). Russian Journal of Plant Physiology. 2008 Oct;55(6):843–845.

68. De-Regil L, Jefferds M, Sylvetsky A, Dowswell T. Intermittent iron supplementation for improving nutrition and development in children under 12 years of age (Review). The Cochrane Library. 2011; Issue 12: .

69. Blaby-Haas CE, Merchant SS. Lysosome-related organelles as mediators of metal homeostasis. Journal of Biological Chemistry. 2014; 289(41):28129–28136. doi: 10.1074/jbc.R114.592618 PMID: 25160625

70. Claus J, Chavarría-Krauser A. Modeling regulation of zinc uptake via ZIP transporters in yeast and plant roots. PLOS ONE. 2012; 7(6):e37193. doi: 10.1371/journal.pone.0037193 PMID: 22715365

71. Alon U. An Introduction to Systems Biology. Design Principles of Biological Circuits. London: CRC press; 2006.

72. Louie AH. Robert Rosen's anticipatory systems. Foresight. 2010; 12(3):18–29. doi: 10.1108/14636681011049848

73. Rosen R. Anticipatory systems. New York: Springer; 2012.

74. Moore-Ede MC, Sulzman FM, Fuller CA. The clocks that time us. Cambridge, Massachusetts: Harvard University Press; 1982.

75. Moore-Ede M. Physiology of the circadian timing system: Predictive versus reactive homeostasis. Am J Physiol. 1986; 250:R737–52. PMID: 3706563

76. Duc C, Cellier F, Lobréaux S, Briat JF, Gaymard F. Regulation of iron homeostasis in Arabidopsis thaliana by the clock regulator time for coffee. Journal of Biological Chemistry. 2009; 284(52):36271–36281. doi: 10.1074/jbc.M109.059873 PMID: 19828447